JNK2 pathway in colonocytes enhances gut barrier integrity in response to microbial acetate.

Chen Chongtham[1], Trisha Biswas[1,#], Namaste Kumari[1,#], Raunak Kar[2], Jyotsna [3], Jayalakshmi S[1], Archana Pant[1], Veena S. Patil[2], and Gopalakrishnan Aneeshkumar Arimbasseri[1]*.

[1]Molecular Genetics Laboratory, National Institute of Immunology, New Delhi, India
[2]Immunogenomics Laboratory, National Institute of Immunology, New Delhi, India
[3]Immunometabolism Laboratory, National Institute of Immunology, New Delhi, India
# These authors contributed equally.
*Correspondence: aneesh@nii.ac.in

Corresponding Author:
Gopalakrishnan Aneeshkumar Arimbasseri
Molecular Genetics Laboratory,
National Institute of Immunology,
Aruna Asaf Ali Marg,
New Delhi 110067
Email: aneesh@nii.ac.in
Phone: +91 9971986746

The authors have declared that no conflict of interest exists.

KEYWORDS
Weaning, JNK2 pathway, P38 pathway, Gut microbiome, Colitis inflammation

SUMMARY

The weaning process accompanies changes in the nutritional profile, metabolism, and gut immune tolerance of offspring. However, the molecular changes associated with this transition and their implications for gut health are not well understood. Here, we show that post-weaning milk-based diets modulate the gut microbiome of pups by enriching *Dubosiella newyorkensis.* This, in turn, enhances gut barrier function by activating the JNK2 pathway in the epithelium through acetate. However, an inflammation-inducing lard-based high-fat diet, a brief pharmacological inhibition of JNK2, or a two-week delay in the initiation of milk-based diets post-weaning leads to the activation of P38 in the epithelial cells, which leads to inflammation. These observations reveal a microbiome-dependent, short-chain fatty acid-driven dichotomy between JNK2 and P38 pathways in the gut epithelium that modulate gut inflammation. These results provide a framework connecting diets, microbiome, and molecular changes in the epithelium, which may aid the design of microbiome-directed dietary interventions.

43 **INTRODUCTION**

44 The diet-microbiome-host axis in the gut has emerged as a key factor in chronic diseases,
45 including inflammatory bowel diseases, metabolic and cardiovascular diseases, and
46 cancer. While several diets, such as the Mediterranean diet, fermented food, and high-
47 fiber diet, have been considered microbiome-friendly, others, including high-fat and
48 Western diets, promote an unhealthy microbiome, leading to gut inflammation (Perler,
49 Friedman et al. 2023). Microbiome-directed dietary interventions have been shown to be
50 an effective tool to fight childhood malnutrition (Blanton, Charbonneau et al. 2016).
51 However, to formalize the nature of different diet-microbiome-gut interactions and to
52 develop novel strategies for intervention, it is essential to identify the molecular signatures
53 and mechanisms that drive such interactions.

54 Weaning represents an important metabolic transition in mammals, where the pups stop
55 milk intake and depend completely on solid food. Adolescence, which follows the weaning
56 (3-7 weeks in mice), is also an important period of active growth and susceptibility to
57 malnutrition. Milk exhibits higher fat content (Ballard and Morrow 2013), while post-
58 weaning diets are primarily carbohydrate-based in most of the populations. This shift
59 leads to the metabolic maturation of mammals to adapt to staple diets. In rodents, during
60 weaning, the liver reduces gluconeogenesis and increases carbohydrate storage and
61 utilization (Ferré, Decaux et al. 1986, Kalhan and Parimi 2000). Similarly, a shift from
62 mTORC1 activation to AMPK activation in pancreatic islets during weaning is essential
63 for islet maturation and glucose-induced insulin secretion (Stolovich-Rain, Enk et al. 2015,
64 Jaafar, Tran et al. 2019). Mice lacking the vitamin D receptor tend to develop severe

growth defects upon weaning, characterized by their inability to utilize carbohydrates (Das, Gopinath et al. 2022). However, subjecting these mice to milk-based diets upon weaning led to the restoration of growth and energy metabolism in these mice, indicating specific nutritional requirements after weaning (Das, Jawla et al. 2023). Furthermore, milk has been shown to affect nutrient absorption in the intestine as well (Song, Kato et al. 2003).

Unlike most other animals, humans continue consumption of milk and milk products even after weaning. Indeed, dairy products are major sources of healthy nutrition for humans. However, very little is known about the effect of continued milk supplementation post-weaning on gut function. While patients with inflammatory bowel disease tend to exclude milk and milk products, conflicting conclusions have been made on the effect of milk and dairy products on gut inflammation (Opstelten, Leenders et al. 2016, Narula, Wong et al. 2021, Kempinski, Arabasz et al. 2024). Gut-microbiome diversity and function change with diets and the variation in the gut microbiome could be one of the driving forces that determine the positive and negative effects of milk on gut health. During the postnatal period, several milk components, including Immunoglobulin A, complex oligosaccharides, higher fat content, etc., are essential for developing a healthy microbiome (Xu, Zhou et al. 2024). The weaning period is one of the most important stages of microbiome maturation in mammals, with the changes in microbiota during this period having long-lasting effects on gut and metabolic health (Al Nabhani, Dulauroy et al. 2019, Barratt, Nuzhat et al. 2022, Paredes, Justo-Mendez et al. 2023). During the weaning period, the changes in the diet lead to rearrangement of the gut microbiome, which is associated with

87 a spike in inflammation followed by its resolution (Al Nabhani, Dulauroy et al. 2019). This
88 'weaning reaction' is essential for the development of immune tolerance towards the
89 altered microbiome. Interrupting this process leads to increased susceptibility to DSS-
90 induced gut inflammation (Al Nabhani, Dulauroy et al. 2019).

91 Host-microbiome interactions are controlled by a multitude of factors, including microbial
92 metabolites, including short-chain fatty acids, host-secreted proteins such as
93 antimicrobial peptides, metabolites, dietary components, etc. (Wilde, Slack et al. 2024).
94 The mechanisms by which these metabolites enhance gut barrier function or lower
95 pathological inflammation are not completely understood. JNK and P38 pathways are
96 among the core signaling pathways in mammalian physiology, regulating various
97 processes such as cell proliferation and inflammation. In the gut, both these pathways
98 are known to affect inflammation, gut barrier function, epithelial regeneration, and cancer
99 (Roy, Rashid et al. 2008, El Abbas, Radermecker et al. 2020, Canovas and Nebreda
100 2021). AP-1 transcription factors are one of the major classes of targets for the JNK
101 pathway, which are known to regulate gut regeneration and cancer. JNK pathway was
102 shown to enhance epithelial regeneration by enhancing WNT signaling (Sancho, Nateri
103 et al. 2009). Deletion of MBD3, an inhibitory protein associated with unphosphorylated c-
104 Jun, leads to enhanced progenitor proliferation (Aguilera, Nakagawa et al. 2011, Zhang,
105 Pronovost et al. 2024). Genetic depletion experiments have shown that JNK2, but not
106 JNK1, enhances gut barrier function and protection against dextran sodium sulfate
107 treatment (DSS) (Mandic, Bennek et al. 2017). However, another study has shown that
108 osmotic stress-induced activation of JNK2 deteriorates tight junction protein expression

109 and gut barrier function (Samak, Suzuki et al. 2010), indicating the context-dependent
110 effects of JNK2 activation in the gut epithelium. While P38 activation leads to upregulation
111 of pro-inflammatory cytokines, it also works downstream to the cytokine signaling
112 pathways to further enhance inflammation (Parhar, Ray et al. 2003). However, how these
113 two important pathways are regulated in different contexts of gut inflammation is
114 unknown.

115 To delineate the effects of post-weaning milk consumption, we analyzed pups fed on milk-
116 based diets either immediately after weaning or two weeks after weaning. We show that
117 mice weaned onto milk-based diets maintain gut epithelial integrity even after a challenge
118 with 1.5% DSS for 7 days, while a 2-week delay in the introduction of these diets caused
119 opposite effects. Molecular analysis reveals a complex liaison between the gut
120 microbiome and the epithelial cells, which protects the epithelial layer from DSS insult,
121 with the dichotomy between epithelial JNK2 and P38 pathways being the deciding factor
122 in pathological inflammation. We identified *D. newyorkensis* generated acetate mediates
123 activation of JNK2 to protect gut barrier function.

124

125 # RESULTS

126 **Post-weaning milk-based diets protect from DSS-induced gut inflammation.**

127 To address the effect of an extended milk-like diet on gut health, we weaned the pups
128 onto two different milk-based diets at the age of 3 weeks: a custom-designed, milk-fat-
129 based diet (MFD) mimicking milk composition or a commercial milk-based formula
130 Lactogen 2 (MBD) containing 54.8% milk solids. The macronutrient composition of these
131 two milk-based diets varies, with MFD exhibiting higher fat content while Lactogen 2 has
132 higher carbohydrate content. (Supplementary Table 1, Figure S1A). These diets were
133 shown to rescue growth defects in mice lacking the vitamin D receptor (Das, Jawla et al.
134 2023). We also included a lard-based high-fat diet (HFD) to distinguish the effect of high-
135 fat content from the effect of milk components in the diet (Supplementary Table 1, Figure
136 S1A). HFD is well-established to induce gut inflammation (Duan, Zeng et al. 2018). Mice
137 were subjected to these diets or regular chow diet (RCD) for 4 weeks, followed by
138 treatment with 1.5% DSS for 7 days to induce inflammation (Figure 1A).

139 Disease severity score calculated from stool consistency and rectal bleeding shows that
140 both MBD and MFD-fed mice exhibit delayed onset of these disease symptoms; the
141 severity is significantly lower for these groups at the end of the experiment (Figure 1B).
142 In contrast to both the RCD and HFD-fed mice, the reduction in body weight during the
143 DSS challenge was also lower for MBD and MFD-fed mice (Figure 1C). Though DSS
144 treatment led to a reduction in colon length in all groups, MBD and MFD-fed mice
145 exhibited longer colons compared with both HFD and RCD after DSS treatment (Figure
146 1D& Figure S1B). Histopathology analysis showed that while all groups of mice exhibited

147 cell infiltration in the lamina propria upon treatment with DSS, the RCD-fed and HFD-fed
148 mice exhibited more extensive tissue damage and disintegration of the epithelial layer
149 (Figure 1E). On the other hand, both MBD and MFD-fed mice exhibited well-maintained
150 colonic epithelial architecture. Importantly, HFD-fed mice show cell infiltration even
151 without DSS treatment, suggesting diet-induced inflammation (Duan, Zeng et al. 2018).

152 Further, DSS-treated mice fed on milk-based diets exhibited lower levels of pro-
153 inflammatory cytokine mRNAs *Il1b*, *Tnfa*, and *Il6* compared with the HFD and RCD
154 counterparts, clearly indicating that the inflammatory response is lower in these groups
155 (Figure 1F-H). The anti-inflammatory cytokine mRNAs *Il10* and *Tgfb* showed similar levels
156 of upregulation in RCD and both milk-based diets upon treatment with DSS (Figure
157 S1C&D), indicating that reduced pro-inflammatory signals underlie the protective effect
158 of milk-based diets rather than increased anti-inflammatory activity. On the contrary, the
159 HFD group exhibited lower levels of *Il10* and *Tgfb* mRNAs upon DSS treatment (Figure
160 S1C&D).

161

162 **MBD-fed mice exhibit reduced Immune activation after DSS treatment.**

163 Diet-induced gut inflammation is a complex phenomenon involving the dietary
164 components, microbiome, gut barrier, and the immune compartment. To understand the
165 immune correlates in host immune and epithelial cells subjected to milk-based diets, we
166 performed a single-cell RNAseq analysis of mice fed on MBD or RCD after 7 days of DSS
167 treatment and compared them to untreated controls (Figure S2A). For each condition,
168 cells from three mice were pooled. We sorted epithelial (EpCAM^{+}), B cell (CD45^{+}

169 CD19^{+}), T cell (CD45^{+} CD3^{+}), and non-lymphoid (CD45^{+} CD3^{-} CD19^{-}) cells from the
170 colon (Figure S2B) and mixed (6000 epithelial cells, 2000 B cells, 4000 T cells, and 8000
171 myeloid cells) before subjecting them to GEM generation and library preparation using
172 10X genomics 3′ GEX technology. The scRNA-Seq data was analyzed primarily using
173 the Seurat package (Figure S2C). Epithelial cells (*EpCAM*, *Krt8*, and *Krt18*), B cells
174 (*CD79a*, *Ms4a1*, and *Cd19*), T cells (*Cd3d*, *Cd3e*, and *Cd3g*), and myeloid cells (*Cd14*,
175 *Itgam*, *Fcgr3*, *Itgax*, *H2-Aa*, and *H2-Ab1*) were separated and analyzed (Figure S2C&D).

176 Analysis of B cells showed 17 clusters in three major groups (Figure 2A & Figure S2E).
177 Clusters 1, 2, 3, 12, 15, & 17 constitute IgD and IgM expressing naive B cells, while
178 clusters 4, 5, 9, and 14 constitute plasma cells. The third major group, constituting mostly
179 clusters 0, 6, 8, 13, and 16, shows the expression of IgA, indicating that these are antigen-
180 experienced, class-switched cells, though the IgA expression levels were not as high as
181 in the plasma cells (Figure 2A&B and Figure S2E). The most intriguing effect of diet was
182 observed in the DSS-treated groups. The RCD-DSS group showed very high levels of
183 antigen-experienced, class-switched IgA+ B cells with maximum contribution (37% of
184 total B cells) from cluster 0 (Figure 2A and Figure S2E), suggesting infiltration of antigen,
185 probably due to leaky gut, induced by DSS. IgA expression levels in this cluster are lower
186 than in plasma cells, and they exhibit higher levels of activation markers CD80 and CD44
187 (Figure 2C). On the other hand, in the MBD DSS group, naïve B cells belonging to cluster
188 1 (33% of total B cells) dominated, indicating lower levels of antigen exposure and
189 reduced activation of B cells. Interestingly, even the control mice on MBD showed a
190 higher fraction of cells in cluster 1. Taken together, the RCD-DSS group exhibits higher

191 levels of activated class-switched B cells, while the MBD-DSS group was enriched for
192 naive B cells (Figure S2E), suggesting reduced antigen exposure.

193 T cells from all four conditions formed 17 clusters, with 62% of cells distributed between
194 clusters 0-4 (Figure S2F). Clusters 2, 3, 9, 10, 12, 13, 14, and 16 encompass CD8 cells
195 expressing *Cd8a* and *Cd8b1* (Figure 2D). On the other hand, clusters 0 and 1 exhibit the
196 expression of *Cd8a* without the expression of *Cd8b*. This could be the CD8αα cells
197 observed in the gut (Figure 2D). Clusters 4, 5, 7, 8, 11, and 15 are CD4 cells. Among
198 these, Th1 cells (*Cd4*, *Tbx21*, *Ifng*; cluster 4), Th2 (*Gata3*, *Il13*, *Il4*; cluster 11), Treg cells
199 (*Fox3p*, *Il2r*; cluster 7), and Th17 cells (*Rorc*, *Il17*; cluster 15) could also be identified
200 (Figure 2E). Clusters 2, 10, and 16 represent recently activated (*Cd69*) CD8 (*Cd8a*,
201 *Cd8b1*) cells (Figure 2E). Most of the CD8αβ clusters exhibited expression of *Ifng*, *Gzma*,
202 and *Gzmb*; and cluster 0 of CD8αα cells exhibited high expression of granzymes.
203 However, unlike the B cells, analysis of the distribution of these cells in different conditions
204 showed that they are more or less similarly distributed. An exception was cluster 12,
205 which expresses cytotoxic markers and is highly enriched in the RCD-DSS group but low
206 in the MBD-DSS group. Moreover, cluster 13 is enriched in the DSS-treated groups
207 (Figure 2F). There was a moderate increase in the Th1 (cluster 4) and Treg (cluster 7)
208 populations in MBD-fed mice (Figure 2F). Interestingly, there was a higher percentage of
209 cells from chow-fed control mice in cluster 2, which are activated CD8+ T cells expressing
210 *Cd69* and effector molecules.

211

212 DSS treatment led to major changes in the myeloid cell populations in both MBD and
213 RCD groups (Figure 2G&H). RCD-fed mice exhibited an expansion of CD27 expressing
214 cytotoxic NK cells (cluster 0; *Klrk1*/NKG2D, *Cd7*, *Cd27*, *Gzma*, *Gzmb*, *Prf1*, and death
215 receptor ligands Fasl and Trail) (Hayakawa, Huntington et al. 2006, Hayakawa and Smyth
216 2006) (Figure 2H&I). Apart from the cytotoxic markers, these cells exhibit increased
217 expression of ribosomal protein-coding genes, indicating increased biosynthetic activity
218 (Figure S2G). However, MBD-fed mice treated with DSS showed enrichment of gut-
219 protective macrophages expressing *Mrc1*/CD206 and *Csf1r* (Cluster 2) (Figure S2G) and
220 an increase in the number of monocytes (cluster 3) (Figure 2H) expressing inflammatory
221 cytokines *Il1a*, *Il1b*, *Saa3*, and the cell adhesion molecules *Vim* and *Fn1* (Figure 2J)
222 (Zheng, Wang et al. 2022, Peng, Fang et al. 2024). These results indicate that RCD-fed
223 mice when treated with DSS for 7 days, exhibit higher levels of cytotoxic NK cells, which
224 are part of normal inflammatory response in the gut. However, MBD-fed mice treated with
225 DSS maintain pro-inflammatory monocytes and a homeostatic macrophage population.
226 On the other hand, no significant differences in the cell populations were observed
227 between MBD and RCD under non-DSS conditions. Both groups were enriched in gut-
228 protective macrophages expressing *Mrc1*/CD206 and *Csf1r* (Cluster 2), *Ly6c2* expressing
229 monocytes (Cluster 5), and MHCII expressing cDC2 populations (Cluster 8) (Figure S2H-
230 J and Figure 2G&H).

231 Taken together, the results presented show that MBD-fed mice show a distinct
232 immunological profile characterized by lower levels of antigen-experienced B cells,

233 cytotoxic NK cells, and higher levels of homeostatic macrophages, which reflect reduced
234 immune activation.

235

236 **Milk-based diets maintain gut barrier function even after DSS treatment.**

237 One of the striking observations from the histopathological analysis of the colon was the
238 preservation of the epithelial layer in milk-based diet groups even after 7 days of DSS
239 treatment. Re-clustering of the epithelial cells (Figure S2C &D) resulted in 23 clusters
240 (Figure 3A). Marker analysis identified all major epithelial cell types among these clusters
241 (Figure 3B and Figure S3A-G). The control groups on both diets show similar levels of
242 different cell types (Figure 3B and Figure S3H). The RCD-fed mice treated with DSS show
243 dramatic expansion of cluster 0 (Figure S3B&H), which expresses high levels of
244 inflammatory genes, including *Il1b* & *Tnfa* (Figure 3C and Figure S3I). A similar signature
245 was exhibited by cells in clusters 3, 8, 9, 15, 19, 21, and 22 (Figure 3C and Figure S3I).
246 Previous studies have shown that induction of colitis in mice leads to high expression of
247 *Il1b*, *Tnfa*, and *Cd14* in colonocytes (Meijssen, Brandwein et al. 1998, Waterhouse and
248 Stadnyk 1999). Epithelial cells *in vitro* enhance the expression of *Il1b* when treated with
249 LPS (Waterhouse and Stadnyk 1999). We consider these cells as inflammatory epithelial
250 cells (Figure 3B). Interestingly, these cells are almost exclusively present in the RCD-
251 DSS group, with very low numbers in the MBD-DSS group (Figure 3B and Figures
252 S3H&J), reiterating the reduced inflammation in the latter.

253 On the other hand, the MBD-DSS group exhibited an increased number of colonocytes
254 and preservation of the ISC population (Figure 3B, Figure S3J). Notably, clusters 2, 10,

255 and 11, which belong to colonocytes, are upregulated in the MBD-DSS group compared
256 with the RCD-DSS group (Figure 3A and Figure S3H). A meta-analysis of transcriptomics
257 data from colitic and normal colonic tissue identified a set of 10 marker genes for mucosal
258 barrier repair (Zhao, Zhao et al. 2023). We found that clusters 2, 10, 11, 13, and 18
259 showed increased expression of this gene set, with maximum expression in cluster 10,
260 which is enriched in the MBD-DSS group (Figure 3D). Further analysis of the expression
261 of tight-junction protein-coding genes showed upregulation of *Tjp1*, *Ocln*, *Cldn7*, and *F11r*
262 in these clusters (Figure 3E). Moreover, these clusters exhibited higher expression of
263 transcription factors *Hnf4a* and *Cdx2*, both of which were also established to be
264 associated with gut barrier integrity. To confirm these observations, we performed qRT-
265 PCR analysis of the colon tissues from control and DSS-treated mice (Figure 3F-J). *Tjp1*,
266 *Cldn7*, and *Ocln* mRNAs were upregulated in the MBD and MFD groups treated with DSS
267 compared with RCD-DSS groups. Furthermore, the transcription factor mRNAs *Cdx2* and
268 *Hnf4a* also recapitulated the scRNAseq results. Interestingly, these mRNAs were
269 expressed at lower levels in HFD groups, further supporting their association with gut
270 barrier protection/repair.

271 Further, we asked if the increased expression of tight junction proteins is functionally
272 translated to better barrier function. Indeed, we observed lower levels of FITC-Dextran in
273 the blood 10 minutes after oral gavage in both MBD and MFD-fed mice (Figure 3K). These
274 results clearly show that milk-based diets enhanced the barrier function of the colonic
275 epithelium. Given the delayed onset of symptoms and lower activation of immune cells,

276 we argue that the enhanced barrier function could be underlying the protective effect of
277 milk-based diets.

278

279 **Milk-based diets elicit protective effects against gut inflammation by activating the**
280 **JNK2 pathway in the epithelial cells.**

281 Next, we investigated the mechanisms by which milk-based diets affect intestinal barrier
282 function. We performed the regulome analysis of the scRNAseq data using the SCENIC
283 package (Van de Sande, Flerin et al. 2020). We observed that the clusters that are
284 enriched in the MBD groups – 2, 10, and 11 – showed enrichment of a common set of
285 regulome (Figure 4A and Figure S4A). The transcription factors whose regulome are
286 enriched in these clusters include several AP-1 transcription factors (*Jund*, *Jun*, *Junb*,
287 *Fosl*, *Atf3*, and *Atf4*) and transcription factors well established to have positive effects on
288 gut barrier function (*Hnf4a*, *Nr1i2*/PXR, *Nr1h4*/FXR, *Egr1*) (Dou, Mukherjee et al. 2012,
289 Modica, Cariello et al. 2014, Vemuri, Radi et al. 2023). Transcript levels of each of these
290 transcription factors are also upregulated in these clusters (Figure 4B).

291 AP-1 transcription factors are key players in the regulation of inflammation and epithelial
292 regeneration. Constitutive activation of AP1 transcription factors is known to enhance
293 intestinal stem cell proliferation (Aguilera, Nakagawa et al. 2011). Moreover, a network of
294 different transcription factors identified here, with AP1 as the key factor, is known to
295 modulate gene expression of tight-junction proteins and antimicrobial peptides (Jung,
296 Mangelsdorf et al. 2006, Cattin, Le Beyec et al. 2009, Krueger, Madeja et al. 2009, Chen,
297 Wang et al. 2010, Zhang, Yin et al. 2010, Dou, Mukherjee et al. 2012, Modica, Cariello et

298 al. 2014, Yu, Yang et al. 2022, Wang, Yu et al. 2023) (Figure S4B). Accordingly, our data
299 showed upregulation of the transcripts encoding tight junction proteins in these samples
300 (Figure 3E-H). Moreover, transcripts of antimicrobial peptides *Reg3b* and *Lypd8*, which
301 are known to modulate the gut microbiome to the advantage of hosts, are highly
302 expressed in clusters 2, 10, and 11, along with other colonocyte lineage clusters 13, 17,
303 and 18 (Figure 4C). qPCR analysis of whole colon tissues also showed the transcript
304 levels of these mRNAs are enhanced in the milk-diet groups (Figure 4D&E). However,
305 they were not altered in the HFD group. On the other hand, we observed increased *Cox2*
306 and *Ptges2* mRNAs, which are mediators of inflammation, by enhancing prostaglandin
307 synthesis in the HFD group (Figure S4C&D).

308 MAPK pathways such as ERK, JNK, P38, and several GPCR pathways are known to
309 activate the AP-1 transcription factors. So, we asked if any of these pathways are
310 upregulated by milk-based diets. Interestingly, western blot analysis of the colonic
311 epithelial cells isolated from control mice on different diets (without DSS treatment)
312 showed that milk-based diets induce phosphorylation of JNK2 (Thr183/Tyr185) (Figure
313 4F, asterisk). This indicates that these cells are primed with JNK2 activation even before
314 DSS treatment. On the other hand, HFD, which is associated with increased inflammation
315 in the gut even without DSS treatment, exhibited hyper-phosphorylation P38
316 (Thr180/Tyr182) instead of the JNK2 (Figure 4G, asterisk). These results reveal that gut-
317 protective milk-based diets and inflammation-inducing HFD activate two distinct MAPK
318 pathways in the epithelial cells even in the absence of DSS treatment. We hypothesize

319 that the milk-based diets prime the epithelial cells in the basal state (non-DSS treatment
320 condition) by activating the JNK2 pathway.

321 Next, we asked if activation of JNK2 mediates the protective phenotype elicited by a milk-
322 based diet. To address this, we rectally administered an inhibitor of JNK (JNK inhibitor II;
323 SP600125) at 10μg/g body weight. This treatment led to the downregulation of JNK2 in
324 the colonic epithelium even after 24 hours of treatment (Figure S4E). So, we treated MFD-
325 fed mice with the JNK2 inhibitor 24 hours prior to DSS exposure. At 7 days post DSS
326 treatment, the inhibitor-treated, MFD-fed mice exhibited higher disease severity, loss of
327 body weight, and reduced colon length compared with the vehicle-treated group (Figure
328 4H-J, Figure S4F). Interestingly, the disease severity was higher even in RCD-fed mice
329 treated with JNK2 inhibitor as well, supporting the conclusion that even the basal JNK2
330 observed in RCD plays a beneficial role. Histopathology analysis confirmed that the JNK
331 inhibition led to increased pathology in the MFD group (Figure S4G). The mRNA levels
332 of pro-inflammatory cytokines TNFα and IL1β were upregulated in the JNK2 inhibition
333 groups, indicating higher levels of inflammation (Figure 4K). Furthermore, the barrier
334 protection-associated genes *Muc2*, *Tjp1*, *Ocln*, and *Hnf4a* also show decreased
335 expression, suggesting that the JNK2 pathway controls the expression of these mRNAs
336 (Figure 4L & Figure S4H). The mRNA levels of AMPs LYPD8 and REG3b in the colonic
337 tissue were also downregulated (Figure 4M) by JNK inhibition.

338 We also found that the inhibition of JNK2 was observed even after 7 days in the MFD-fed
339 mice without DSS treatment (Figure S4I). This inability to restore the JNK2 suggests that
340 once it was inhibited, the dietary intervention failed to reactivate it. Interestingly, inhibition

341 of JNK2 led to increased phosphorylation of P38, which corroborates with the increased
342 disease severity in the inhibitor-treated groups (Figure 4N). These results emphasize the
343 dichotomy of JNK2 and P38 pathways in colon inflammation.

344

345 **A break in the milk-based diet regimen alleviates JNK2 phosphorylation and**
346 **protective effects.**

347 Next, we asked if the milk-based diets can extend their protective effect against repeated
348 DSS challenges. To address this, we subjected these mice to a second round of DSS
349 treatment after recovering for two weeks from the first round (Figure 5A). Interestingly,
350 the disease severity scores, body weight changes, colon length, and pro-inflammatory
351 cytokine levels showed that mice weaned onto MFD exhibited reduced inflammation even
352 on repeated DSS challenges (Figure 5A-E; MFD(I&II)). However, initiating the MFD
353 feeding after the first round of DSS treatment of RCD-weaned mice failed to show a
354 protective effect (Figure S5A-C; RCD(I)-MFD(II)), suggesting that though milk-based
355 diets can provide long-term protection from DSS-induced inflammation, this protective
356 effect is lost once regular chow feeding is initiated. These results and the inability of MFD
357 to reactivate JNK2 after one round of inhibition (Figure S4I) suggest that the continuity of
358 MFD is necessary to maintain gut barrier function.

359 To further confirm this, we subjected mice to a milk-based diet two weeks after weaning
360 them onto RCD (RCD-MFD feeding) (Figure S5D). When we subjected these mice to
361 DSS treatment, RCD-MFD-fed mice exhibited loss of weight, colon length reduction, and
362 disease severity comparable with the chow-fed mice (Figure 5F-H). Histopathology

363 analysis of the colon also showed increased pathology in these mice (Figure 5I). Pro-
364 inflammatory cytokine mRNAs *Il1b*, *Ifng*, and *Tnfa* were also upregulated in the whole
365 colon tissue, indicating increased inflammatory response (Figure 5J). Further, we
366 specifically analyzed the epithelial compartment without DSS challenge to see the basal
367 expression of the tight junction proteins and anti-microbial peptides (*Reg3b* and *Lypd8*)
368 and found them to be downregulated in the RCD-MFD group compared with the MFD
369 group (Figure 5K&L). These results clearly show that when a break was introduced in
370 milk-based diets, the signature changes associated with a protective milieu were
371 abolished.

372 Further, we found that, unlike the MFD group, the RCD-MFD group did not show
373 upregulation of JNK2 phosphorylation (Figure 5M), but they showed upregulation of P38
374 phosphorylation (Figure 5N). These data clearly indicate that a break in the milk-based
375 diet feeding fails to activate JNK2 and alleviate its protective effect; instead, it activates
376 the pro-inflammatory P38 pathway. It also reinstates the dichotomy between the JNK2
377 and P38 activation in gut inflammation.

378

379 ***Dubosiella Newyorkensis*, enriched in the milk-based diet groups, provides gut**
380 **protection.**

381 Milk components are known to affect the gut microbiome (Butler, Bastiaanssen et al.
382 2020, Shuai, Zuo et al. 2021). The changes in the expression levels of several
383 antimicrobial peptides in mice fed on milk-based diets also point toward the modulation
384 of gut microbiome by milk-based diets. To test whether any of the protective correlates of

385 the milk-based diets are due to the gut microbiome, we removed the microbial flora from
386 these mice by treatment with a cocktail of antibiotics (Vancomycin (0.5 mg/ml), Ampicillin
387 (1 mg/ml), Neomycin (0.5 mg/ml), and Metronidazole (0.625 mg/ml) in 2% sucrose)
388 (Figure 6A & Figure S6A). When milk-based diet-fed mice were treated with antibiotics,
389 the epithelial JNK2 phosphorylation was reduced significantly compared with MFD
390 without antibiotics (Figure 6B). Interestingly, the genes that were associated with
391 protection, such as the transcription factor *Hnf4a* and the AMPs *Reg3b* and *Lypd8,* were
392 downregulated to that of the RCD group in the MFD-ABX group (Figure 6C&D), indicating
393 clearly that the microbiome plays an important role in the expression of protective markers
394 in milk-based diet groups.

395 Similarly, the P38 activation was also reduced in HFD-fed mice when treated with
396 antibiotics (Figure S6B). mRNA levels of genes downstream to P38, such as *Cox2* and
397 *Ptges2*, and *Tnfa*, a pro-inflammatory cytokine, were also reduced in the HFD group
398 treated with antibiotics (Figure S6C). In addition, the lower levels of tight junction protein
399 and mucin expression observed in HFD-fed mice were restored by antibiotic treatment
400 (Figure S6D). This supports the previous observations that in HFD-fed mice, an altered
401 microbiome is the primary inducer of inflammation (Cani, Amar et al. 2007, Hildebrandt,
402 Hoffmann et al. 2009, Suriano, Vieira-Silva et al. 2023). These results indicate that, as in
403 the case of the hyperinflammation induced by HFD, the protective effect of MFD is also
404 dependent on the microbiome.

405 Next, we analyzed the composition of the gut microbiome by 16s rRNA sequencing using
406 the Oxford Nanopore platform. Interestingly, even though both MFD and MBD showed

407 protection against the DSS-induced pathology, they exhibited little similarity in terms of
408 microbial composition. MBD showed the highest alpha diversity among the groups, while
409 both MFD, HFD, and RCD-MFD groups exhibited lower alpha diversity, suggesting that
410 the overall diversity is affected mostly by the macronutrient content of the diets (Figure
411 6E and Figure S6E). Furthermore, the Chao index also indicated divergent bacterial
412 composition among the MFD and MBD (Figure 6F). Differentially enriched microbes in
413 different diet groups show that both MBD and MFD have increased protective species in
414 the microbiome, while HFD shows increased levels of known pathogenic bacteria
415 (Supplementary Table 3).

416

417 Despite the difference between MBD and MFD in the overall composition of the
418 microbiome, we observed that *Dubosiella newyorkensis* is one of the most abundant
419 species in both groups (Figure 6G&H and Figure S6F-H). *D. newyorkensis*, which is a
420 mouse homolog of the human symbiont *Clostridium innocuum*, has been recently shown
421 to elicit gut protective properties (Zhang, Tu et al. 2024). To address if *D. newyorkensis*
422 indeed mediates the protective effects of MBD and MFD, we subjected the mice to oral
423 treatment with *D. Newyorkensis* for 2 weeks, followed by DSS treatment (Figure S6I).
424 They exhibited protection from DSS-induced inflammation as evidenced by reduced
425 disease severity score, maintenance of body weight, and colon length (Figure 6I-K). The
426 histopathology analysis also shows that there is decreased tissue damage upon
427 treatment with DSS in the *D. newyorkensis* group (Figure S6J).

428 These data clearly show that *D. newyorkensis* protects mice from DSS-induced colitis.
429 We next checked the protective correlates we observed in the milk-based diet groups
430 (Figure 6L-N). The mRNA levels of pro-inflammatory cytokines TNFα and IL1β were
431 reduced in the *D. newyorkensis* group, while the transcripts for the barrier-protective
432 proteins CLDN7, OCLN, TJP1, MUC2, and HNF4α were upregulated as seen in milk-
433 based diet groups (Figure 6M & Figure S6K). Apart from the low inflammatory genes and
434 high gut barrier protection associated genes, the transcript levels of anti-microbial protein
435 transcripts *Reg3b* and *Lypd8* were upregulated in the *D. newyorkensis* treated group
436 (Figure 6N). These results clearly show that *D. newyorkensis* recapitulates salient
437 features of milk-based diets in protection against gut inflammation. Moreover, western
438 blot analyses of the epithelial cells show that phospho-JNK2 is indeed upregulated in the
439 *D. newyorkensis* treated group (Figure 6O & Figure S6L). On the other hand, we did not
440 observe any difference in the p-P38 levels, suggesting that *D. newyorkensis* is sufficient
441 to selectively upregulate the JNK2 pathway in the colonic epithelium (Figure 6O & Figure
442 S6L) and enable the protection from DSS-induced inflammation. Interestingly, the MFD
443 feeding after 2 weeks of RCD failed to enhance *D. newyorkensis* levels, and it was
444 reflected by heightened inflammation in this group (Figure 6G & H and Figure 5).

445

446 **Acetate induces the JNK2 pathway in the colonic epithelium to enhance gut barrier**
447 **function.**

448 Short-chain fatty acids are major contributors toward gut barrier integrity (Lewis,
449 Lutgendorff et al. 2010, Deleu, Arnauts et al. 2023). Milk is a rich source of short-chain

450 fatty acids, especially butyrate and acetate (Barman, Gio-Batta et al. 2024, Wu, Wang et
451 al. 2024). Moreover, *D. newyorkensis* also produces short-chain fatty acids (Zhang, Tu et
452 al. 2024). We performed GC-MS analysis of fecal samples of mice subjected to RCD,
453 MFD, HFD, and RCD-MFD to quantify different short-chain fatty acids. Compared with
454 RCD, we found that acetate, propionate, and butyrate are high in the fecal samples in
455 MFD-fed mice (Figure 7A). On the other hand, in HFD-fed mice, all three of these short-
456 chain fatty acids were low, clearly showing that these short-chain fatty acid levels are
457 indeed correlated with gut protection against DSS treatment. Interestingly, in the RCD-
458 MFD group, which does not show gut-protective phenotype, both acetate and propionate
459 were reduced, while butyrate levels were not significantly lower compared with MFD
460 (Figure 7A). Interestingly, fecal samples of mice treated with *D. newyorkensis* also
461 exhibited higher levels of acetate compared with control samples (Figure 7B). On the
462 other hand, propionate and butyrate did not show a statistically significant increase in
463 these mice (Figure S7A). This data suggests that acetate could be the driving force
464 behind the protective phenotype.

465 Acetate has been shown to protect against DSS-induced colitis previously; however, the
466 mechanism was not known (Laffin, Fedorak et al. 2019, Deleu, Arnauts et al. 2023). To
467 test if acetate treatment functions through JNK2 phosphorylation, we provided potassium
468 acetate to these mice in drinking water (200mM). Indeed, we found that acetate treatment
469 provided protection against DSS-induced pathologies based on body weight, colon
470 length, and disease severity score (Figure 7C-E & Figure S7B). The mRNA levels of pro-
471 inflammatory cytokines TNFα, IL1β, and IFNγ were also significantly downregulated in

472 the acetate-treated group, suggesting reduced inflammation (Figure 7F). Moreover, we
473 observed increased mRNA levels of tight junction protein OCLN, mucin gene MUC2, and
474 the transcription factor HNF4α, which were all associated with MFD feeding in these mice
475 (Figure 7G). Histopathology analysis also shows a well-preserved epithelium in the
476 acetate-treated group, indicating reduced inflammation and improved barrier function
477 (Figure 7H). Next, we asked if acetate enhances protection through the JNK2 pathway,
478 as observed for milk-based diets and *D. newyorkensis*. Indeed, acetate treatment was
479 sufficient to induce JNK2 phosphorylation in the epithelium, while it did not have any effect
480 on P38 phosphorylation (Figure 7I & Figure S7C). Similarly, the mRNA levels of AMPs
481 REG3b and LYPD8 were also upregulated in the acetate-treated group (Figure 7J).

482

483 Taken together, these results show that post-weaning milk-feeding supports the
484 expansion of the *D. newyorkensis* population to increase short-chain fatty acid production,
485 which in turn activates the epithelial JNK2 pathway to enhance gut barrier function. On
486 the other hand, P38 activation is associated with diets that induce chronic inflammation
487 in the gut.

488

489

490 **DISCUSSION**

491 While milk and dairy products are important nutritional ingredients, the effect of milk on
492 gut health after weaning has been poorly understood. Milk and gut inflammation have a
493 contentious relationship in adults. Milk and milk products remain one of the most
494 commonly excluded dietary ingredients by patients with inflammatory bowel disease
495 (Opstelten, Leenders et al. 2016, Narula, Wong et al. 2021, Kempinski, Arabasz et al.
496 2024). However, clinical studies have not yielded an unequivocal conclusion on the
497 adverse or protective effects of dairy (Opstelten, Leenders et al. 2016, Ulven, Holven et
498 al. 2019). Some of the discrepancies in the clinical studies could be induced by the
499 microbiome.

500 This study reveals a complex relationship between diet, gut-microbiome, intestinal barrier,
501 and inflammation shaped by post-weaning consumption of dairy. Continued feeding of
502 the pups with milk-based diets after weaning enhances gut barrier function upon DSS
503 treatment, as evidenced by the maintenance of the gut epithelium in the milk-based diet-
504 fed mice compared with RCD or HFD-fed mice. The key molecule that drives gut
505 protection is the short-chain fatty acid acetate, produced presumably by the microbiome,
506 especially *D. newyorkensis*. Acetate, like other short-chain fatty acids, is known to
507 enhance gut protection in similar models; however, the pathways by which it mediates
508 protection were not well understood. Here, we show that acetate activates the JNK2
509 pathway to elicit its gut protective function.

510 Dietary modulation of the healthy microbiome is a promising strategy to address various
511 conditions ranging from malnutrition to chronic disorders (Chen, Mostafa et al. 2021,

512 Mostafa, Hibberd et al. 2024). Because the diet-microbiome-inflammation relationship is
513 indeed complex, the development of such strategies requires a framework based on the
514 associated molecular mechanisms. This is indeed important as the same diet could
515 induce different outcomes based on the gut microbiome composition, as exemplified by
516 the RCD-MFD group in this study. Here, at least three features of gut protection by milk-
517 based diets are identified in the host: Upregulation of JNK2 phosphorylation in the
518 colonocytes, upregulation of gut barrier protection genes such as tight junction proteins,
519 and the expression of antimicrobial proteins Reg3b and Lypd8. JNK2 and its downstream
520 targets, AP-1 transcription factors, are known to promote epithelial cell proliferation,
521 epithelial repair, and regeneration, which corroborates our data (Roy, Rashid et al. 2008,
522 Sancho, Nateri et al. 2009, Aguilera, Nakagawa et al. 2011, Mandic, Bennek et al. 2017,
523 Wang, Wang et al. 2017). Tight junction proteins are essential in the maintenance of the
524 gut epithelial barrier and are known to be upregulated by activation of transcription factors
525 such as AP-1, HNF4α and CDX2, which are also upregulated by milk-based diets
526 (Coskun, Troelsen et al. 2011, Vemuri, Radi et al. 2023). The third characteristic of
527 epithelial protection was the antimicrobial peptides. Both REG3B and LYPD8 are the
528 predominant AMPs expressed in the colon; on the other hand, a wider array of AMPs is
529 expressed in the proximal intestine. Reg3b and Lypd8 are gut protective as their deletion
530 induces gut inflammation (Shindo, Katagiri et al. 2020, Hsu, Okumura et al. 2021). Both
531 Reg3b and Lypd8 affect only a sub-population of microbes (Okumura, Kurakawa et al.
532 2016, Wang, Fouts et al. 2016).

533 Interestingly, all these changes are affected by antibiotic treatment, suggesting that the
534 protective effects are due to microbial products rather than a direct effect of dietary
535 components on host cells. In support of this, all three features were restored when the
536 mice were treated with *D. newyorkensis*. *D. newyorkensis* has been shown to enhance
537 gut protection recently (Zhang, Tu et al. 2024). The proposed mechanisms include
538 immune modulation by maintaining Th17/Treg balance. Lysine produced by *D.*
539 *newyorkensis* was shown to achieve immune tolerance by activating the kinurenin
540 pathway in dendritic cells. Our data also showed that the protective myeloid populations
541 were preserved in the MBD-fed mice treated with DSS but emphasized the effect of this
542 bacterium on the epithelial cells. The data presented advances the function of *D.*
543 *newyorkensis* to enhance gut barrier function by activating the JNK2 pathway in the
544 epithelium through acetate. Though acetate and other short-chain fatty acids have been
545 shown to be gut-protective, their requirement for JNK2 activation was not known. Further,
546 the data indicates that continued dairy consumption post-weaning is a natural mechanism
547 to enhance the *D. newyorkensis* population in the gut, thus an example of microbiome-
548 directed food.

549 JNK and P38 pathways are two core signaling pathways that control cell physiology,
550 including cell proliferation, stress response, and inflammation(Roy, Rashid et al. 2008,
551 Canovas and Nebreda 2021). These pathways are well studied in the immune cells in the
552 context of gut inflammation, and the JNK pathway has been shown to affect gut barrier
553 function (Parhar, Ray et al. 2003, Roy, Rashid et al. 2008, Sancho, Nateri et al. 2009,
554 Aguilera, Nakagawa et al. 2011, Mandic, Bennek et al. 2017). However, natural methods

555 to modulate their functions to alleviate pathological gut inflammation were not known.
556 Here, we suggest that these two pathways balance gut barrier integrity and inflammation.
557 Milk-based diets, *D. newyorkensis*, and acetate activate JNK2 and reasonably maintain
558 gut epithelial integrity even after a challenge with DSS for 7 days. On the other hand,
559 feeding HFD, which induces low-grade inflammation even in the absence of any DSS
560 challenge, leads to the activation of P38 in the epithelial cells. The RCD-MFD group,
561 which showed signs of inflammation even in the absence of DSS, also exhibited higher
562 P38 and lower JNK2 phosphorylation. Moreover, inhibition of JNK activity upregulated
563 P38 phosphorylation and alleviated the protective effects of milk-based diets, indicating
564 that these pathways antagonize each other. Thus, we conclude that the relative levels of
565 these pathways in the colonocytes define susceptibility to pathological inflammation in
566 the gut. However, the mechanism by which acetate activates JNK2 phosphorylation
567 remains to be elucidated.

568 The host controls the microbiome by secreting various molecules, including IgA, AMPs,
569 and mucins (Wilde, Slack et al. 2024). The microbiome controls the host and the microbial
570 ecology by secreting various metabolites, antimicrobial peptides, etc (Liu 2023). In the
571 current experimental setup, we observed a possible modulation of the microbial
572 ecosystem by itself but mediated through host-secreted AMPs. The milk-based diets, *D.*
573 *newyorkensis*, and acetate treatment led to the upregulation of AMP genes *Reg3b* and
574 *Lypd8,* which target specific groups of microbes. However, antibiotic treatment abolished
575 the effect of diet on the AMP expression, clearly suggesting the microbial dependence of
576 their activation. Also, the lower expression of AMP coding genes in the RCD-MFD group,

577 where the microbial flora was different from the MFD group, suggests that the
578 establishment of *D. newyorkensis* in the ecosystem as a predominant species would
579 require induction of AMPs by the epithelial cells. The association of milk-based diets and
580 *D. newyorkensis* treatment with AMP expression suggests that the abundance of *D.*
581 *newyorkensis* could be determined by the feed-forward mechanism induced by this
582 bacterium, mediated by AMPs, a process missing in the RCD-MFD group. This
583 hypothesis needs to be tested in gene knock-out models of these AMPs.

584 In short, our data indicate that the modulation of the microbiome from the early post-
585 weaning days by dietary modulation can have long-lasting effects on gut inflammation.
586 More importantly, we also show the effect of diets on the microbiome and inflammation
587 depends on the pre-existing metabolic milieu and microbiome composition. These results
588 are more relevant considering the association between malnutrition and dysbiosis and
589 the effectiveness of early-life microbiome management in addressing growth defects
590 associated with malnutrition (Blanton, Charbonneau et al. 2016, Barratt, Nuzhat et al.
591 2022).

592

593 **CONCLUSIONS**

594 In conclusion, our data shows that continued milk supplementation after weaning has
595 positive effects on the gut epithelium. This enables the establishment of a microbial
596 ecosystem characterized by an increased abundance of *D. newyorkensis*, which
597 produces short-chain fatty acids. We also show that the JNK2 and P38 pathways
598 antagonize each other during the onset of inflammation. While activation of JNK2 is

599 essential for enhanced gut epithelial integrity by acetate, P38 activation is associated with
600 increased inflammation. Inhibition of the JNK pathway is sufficient for the activation of
601 P38 in the gut epithelium.

602

603

604

605

606

607 **MATERIALS AND METHODS**

608 **Materials.**

609 Chemicals, reagents, kits, strains and software used this study are given in tables 1-6.

Table 1: Chemicals and Reagents		
REAGENT or RESOURCE	**SOURCE**	**IDENTIFIER**
AMPICILIN SODIUM SALT	Sigma-Aldrich	A9518
AMPure® XP beads	Beckman Coulter	A63881
Brucella Agar base with Hemin	Himedia Laboratories	M1039
Cell strainer pore size 40um	Himedia Laboratories	TCP024
Cell strainer pore size 70um	Himedia Laboratories	TCP025
Chemiluminescent Substrate	Genaxy	XLS070,0250
Collagenase IV	ThermoFisher	17104-019
Dextran sulfate sodium salt	MP Biomedicals	160110
Dispase	Himedia Laboratories	TC303-100MG
DL-Dithiothreitol	Sigma-Aldrich	43819
EDTA, disodium salt	Bio Basic	EB0185-500
FBS	Gibco	10270-106
FITC-Dextran 4	Sigma-Aldrich	46944
HEPES	Sigma-Aldrich	7365-45-9
METRONIDAZOLE	Sigma-Aldrich	M3761
Modified Tryptone Glucose Meat extract (MTGE) broth	Himedia Laboratories	M1116
NEOMYCIN SULPHATE	Sigma-Aldrich	N6386
JNK inhibitor II	Sigma-Aldrich	SP600125
PBS	Gibco	70011069
Pierce BCA Protein Assay Kit	ThermoFisher	23225
PolyFreeze Tissue Freezing Medium	Sigma-Aldrich	SHH0026
Potassium acetate	MP Biomedicals	02194843-CF
Protease/Phosphatase Inhibitor	Cell signaling	5872
PVDF Transfer Membranes	ThermoFisher	88520
RIPA lysis buffer	Sigma-Aldrich	R0278
RPMI 1640 medium	Gibco	61870036
SUCROSE	Sigma-Aldrich	S0389
Tween 20	Sigma-Aldrich	8.22184.0521
VANCOMYCIN HYDROCHLORIDE	Sigma-Aldrich	V2002

610

Table 2: Antibodies			
Western Antibodies			
REAGENT or RESOURCE	**SOURCE**	**IDENTIFIER**	**DILUTION**
p38 Antibody	CST	8690	1/1000

phospho-p38 Antibody	CST	4511	1/1000
SAP/JNK Antibody	CST	9252	1/1000
phospho-SAP/JNK Antibody	CST	4668	1/1000
Beta-actin Antibody	CST	4967	1/1000
Peroxidase AffiniPure™ Goat Anti-Rabbit IgG (H+L)	Jackson ImmunoResearch	AB_2313567	1/10000
FACS Antibodies			
REAGENT or RESOURCE	**SOURCE**	**IDENTIFIER**	**CLONE**	**DILUTION**
FITC anti-mouse CD326 (Ep-CAM) Antibody	BioLegend	118207	G8.8	1/200
APC anti-mouse CD45 Recombinant Antibody	BioLegend	157606	QA17A26	1/200
PE anti-mouse CD19 Antibody	BioLegend	152408	1D3/CD19	1/200
PE/Cyanine7 anti-mouse CD3 Antibody	BioLegend	100220	17A2	1/200
TruStain FcX™ PLUS (anti-mouse CD16/32) Antibody	BioLegend	156603	S17011E	1/1000

611

Table 3: Commercial kits		
REAGENT or RESOURCE	**SOURCE**	**IDENTIFIER**
NucleoSpin RNA, Mini kit for RNA purification	Macherey-Nagel	740955.5
Primescript cDNA synthesis kit	TAKARA	6110A
SYBR® Premix Ex Taq	TAKARA	RR420A
Pierce BCA Protein Assay Kit	ThermoFisher	23225
Single Cell 3' v3.1 Gel Beads kit	10x Genomics	2000164
16S barcoding kit 1-24	Oxford-Nanopore Technologies	SQK-16S024
Qubit™ dsDNA HS and BR Assay Kits	ThermoFisher	Q32854

612

Table 4: Experimental models: Organisms/strains		
REAGENT or RESOURCE	**SOURCE**	**IDENTIFIER**
Duboisiella newyorkensis	ATCC	TSD-64-0.5ML
Conventional C57BL/6 mice	The Jackson Lab	cat 000664

613

Table 5: Diets		
REAGENT or RESOURCE	**SOURCE**	**IDENTIFIER**
Lactogen 2	Nestle	
Milk Fat Diet	Research Diets	D19112203
High Fat Diet	Research Diets	D12492I
Regular Chow Diet	Altromin	1324

614

Table 6: Software and algorithms		
REAGENT or RESOURCE	**SOURCE**	**IDENTIFIER**
Graphpad Prism v10	GraphPad Prism Inc	https://www.graphpad.com
ImageJ (v. 2.0.0-rc-43/1.51k)	NIH	https://imagej.net

QuantStudio Real-Time PCR software v1.3	Thermo Fisher	https://www.thermofisher.com
FlowJo v10.9.0	BD Bioscience	https://www.flowjo.com
R v4.2.2	R	https://www.r-project.org
Image-Pro Plus 6.0	Media Cybernetics	https://image-pro-plus.software.informer.com
CellRanger Ver: 7.1.0	10x Genomics	https://www.10xgenomics.com
EPI2ME	Oxford Nanopore	https://nanoporetech.com

615

616 **Animal maintenance.**

617 C57BL/6 mice were obtained from Jackson Laboratories (cat.no. 000664) and bred at the
618 small animal facility at the National Institute of Immunology, New Delhi, India. All mice
619 were fed ad-libitum with a commercially available rodent chow (RCD; Altromin; cat.no.
620 1324), a paste of Lactogen-2 (Nestle), formulated milk fat diet (MFD; Research Diets;
621 cat.no. D19112203), high-fat diet/ Western diets (HFD; Research diets; cat.no. D12492I).
622 Mice were housed in the facility in individually ventilated cages (IVC). Animal strain
623 maintenance, post-mortem collection of tissues, drug treatments, and husbandry were
624 carried out according to the guidelines of and with the approval of the Animal Ethics
625 Committee at the National Institute of Immunology.

626 **Dextran sodium sulphate-induced colitis.**

627 24 days old mice were randomly divided into four groups: (1) RCD group, kept with a
628 regular chow diet; (2) MBD group, kept with MBD diet; (3) MFD group, kept with MFD
629 diet; and (4) HFD group, kept with HFD diet. After 28 days of feeding (8-weeks-old mice),
630 each group was divided into two: (a) water with 1.5% DSS; (b) Water without DSS. DSS
631 treatment was done for 7 days. Body weight and disease severity index of mice were
632 recorded daily during the course of treatment (Chawla, Mukherjee et al. 2021). The

633 disease severity score was determined based on stool characteristics and additional
634 symptoms: 0 points for well-formed pellets, 1 point for pasty or semi-formed stool, 2 points
635 for liquid stool, 3 points for stool with a bloody smear, and 4 points for bloody fluid or
636 mortality. Mice experiencing over 30% bodyweight loss were classified as moribund and
637 euthanized. Data from these moribund mice were excluded from the downstream
638 analysis. For the RCD-MFD group, 24-day-old mice were weaned onto RCD, and after
639 2 weeks, MFD feeding was started. For repeated DSS exposure, mice were allowed to
640 recover for 2 weeks after the first round of DSS followed by another round of 1.5% DSS.

641 **Antibiotic treatment.**

642 In experiments where microbiota was removed, a cocktail of antibiotics consisting of
643 Vancomycin (0.5 mg/ml), Ampicillin (1 mg/ml), Neomycin (0.5 mg/ml), and Metronidazole
644 (0.625 mg/ml) in 2% sucrose was orally given to mice from 5 weeks to 7 weeks of ages.

645 **FITC-Dextran cell permeability assay**

646 For assessing intestinal permeability, FITC dextran (0.5 mg/g) was given to the mice 6h
647 prior to analysis of FITC fluorescence in serum. Fluorescence is determined at 510 nm
648 with excitation at 490 nm using the SpectraMax M2 plate reader.

649 **Oral administration of Acetate.**

650 200 mM potassium acetate was given to the 24-day-old mice in their water for three
651 weeks, followed by DSS treatment.

652 **JNK inhibition in colon.**

653 After 24 hours of starvation to clear the colon, the mice were anesthetized with an
654 intraperitoneal (IP) injection of ketamine 100 mg/Kg + xylazine 10 mg/Kg (40 μL/mice). A
655 catheter was carefully inserted into the colon until the tip was 4 cm proximal to the anus.
656 100 μL of JNK inhibitor II (10 ug/g) (SP600125 Merck) in PBS with 10% FBS was
657 administered, and the mice were kept in a Trendelenburg position for 5 min. Mice were
658 allowed to eat *ad libitum*, and 24 hours post inhibitor application, the DSS treatment was
659 initiated.

660 **Administration of *Duboisiella newyorkensis* as probiotic.**

661 D. newyorkensis was obtained from the American Type Culture Collection (ATCC, No.
662 TSD-64-0.5ML) and cultured in modified Tryptone Glucose Meat extract (MTGE) broth at
663 37 °C under anaerobic conditions. The concentration of each bacterium was estimated
664 based on the optical density at 600 nm (OD600). 5-weeks old mice had their microbiomes
665 cleansed by treatment with antibiotic cocktails for two weeks. 100μl of *Duboisiella*
666 *newyorkensis* (1 OD) was then orally administered once in two days for four weeks,
667 followed by DSS treatment.

668 **Histological analysis using Haematoxylin and Eosin staining.**

669 The distal colon tissues were excised from mice after euthanasia. The tissues were
670 washed with ice-cold phosphate-buffered saline (PBS, pH 7.2), embedded in tissue
671 freezing media (Cat SHH00260), and frozen using liquid Nitrogen. Tissues were cut into
672 10-µm-thick sections using a cryotome. The sections were stained with hematoxylin and
673 eosin. Images were captured using Image-Pro6 software on an Olympus inverted
674 microscope under 20X objective.

675 **Intestinal epithelial cell (IEC) isolation.**

676 The mice were euthanized, and the colon was carefully dissected and cut open
677 longitudinally. The tissue was washed three times with PBS, cut into small pieces, and
678 incubated in a pre-digestion buffer (1X PBS with 10 mM EDTA, 0.5 mM DTT) at 37°C with
679 shaking at 200 RPM for 15 minutes. The mixture was centrifuged to remove the pre-
680 digestion buffer, and wash media (RPMI + 5% FBS) was added. The sample was
681 vortexed, and the epithelial cells were collected from the supernatant. The supernatant
682 was then filtered through a nylon cell strainer with a 70-µm pore size.

683 **RNA Isolation and RT-PCR**

684 RNA was isolated from approx. ~0.5 cm of distal colon or IEC using Macherey-Nagel Kit
685 (Cat.no. 740955.50). DNA was removed by treating with DNase from the kit. Purified RNA
686 was quantified using nanodrop (Multiscan SkyHigh) and cDNA was synthesized using
687 Takara cDNA synthesis kit (cat 6110A). qRT-PCR was performed using SYBR® Premix
688 Ex Taq PCR master mix (Takara Cat. # RR420A) in QuantStudioTM 6 Flex Real-Time
689 PCR System instrument. Relative mRNA levels were determined using the 2 -ΔΔCt
690 methods. Actin was used as a control.

691 **Western Blot Analysis**

692 Isolated IECs were lysed using RIPA lysis buffers followed by centrifugation. The protein
693 concentration of the supernatant was checked using BCA. 40µg of total protein was
694 resolved using SDS-PAGE followed by transfer to nitrocellulose membrane. The
695 membrane was probed with primary antibodies against p38 (CST 8690), phospho-p38

696 (CST 4511), SAP/JNK (CST 9252), p-SAP/JNK (CST 4668) and beta-actin (CST 4967).
697 Corresponding secondary antibodies conjugated with HRP and the ECL reagent were
698 used to develop bands. Images were taken using the LAS500 chemidoc system.

699 **Lamina propria immune cell isolation**

700 The mice were euthanized, and the colon was carefully dissected and cut open
701 longitudinally. The tissue was washed three times with PBS, cut into small pieces, and
702 incubated in a pre-digestion buffer (1X PBS with 25 mM HEPES, 10 mM EDTA, 0.5 mM
703 DTT) at 37°C with shaking at 200 RPM for 15 minutes. The mixture was centrifuged to
704 remove the pre-digestion buffer, and wash media (RPMI + 5% FBS) was added. The
705 sample was vortexed, and the epithelial cells were collected from the supernatant. The
706 supernatant was then filtered through a nylon cell strainer with a 70-µm pore size,
707 followed by a second filtration with a 40-µm pore size. The remaining tissue was treated
708 with the digestion buffer (RPMI with 10% FBS, 25 mM HEPES, 0.5 mg/ml Collagenase
709 IV, 0.5 mg/ml Dispase) for 45 minutes at 37°C, with shaking at 200 RPM. The mixture
710 was centrifuged at 1500 RPM for 5 minutes at room temperature, and the supernatant
711 was discarded. Pre-warmed wash media was added, and the sample was vortexed. The
712 supernatant was then filtered through a nylon cell strainer with a 70-µm pore size,
713 followed by a 40-µm pore size, and the cells were counted.

714 **Cell sorting for single-cell RNAseq.**

715 The epithelial cells were pooled with immune cells, and counted the number of live cells
716 using Luna- II Automated Cell Counter. We pooled three mice from each of the groups
717 (RCD with water, Chow with 1.5% DSS, MBD with water, and MBD with 1.5% DSS) in

718 equal numbers. The cells were sorted into four group Epithelial (EPICAM+), B cells
719 (CD45+, CD19+), T cells (CD45+, CD3+), myeloid cells (CD45+, CD3-, CD19+) using
720 BD-FACS Aria sorter. In each group, we pooled 6000 epithelial cells, 2000 B cells, 4000
721 T cells, and 8000 myeloid cells to perform single-cell RNA-Seq using 10X genomic
722 platform.

723 **10X Genomics scRNAseq library preparation**

724 Single cells were partitioned into Gel Beads in Emulsion (GEMs) in the Chromium
725 controller using Single Cell 3' v3.1 Gel Beads kit (10X genomics cat no 2000164) as per
726 the manufacturer's protocol. GEM reverse transcription was performed using PCR
727 condition 53 °C for 45 min, 85 °C for 5 min followed by 4 °C. Post-GEM RT cleanup was
728 performed using Dynabeads MyOne SILANE, and cDNA amplification was performed
729 using PCR condition 98 °C for 3 min, 11 cycles of 98 °C for 15 sec, 63 °C for 20 sec, 72
730 °C for 1 min and 72 °C for 1 min. The cDNA was cleaned up using Ampure XP reagents,
731 followed by fragment analyzer quantification. 3′ gene expression library construction was
732 performed by fragmentation, end repair, and A-tailing double-sided size selection using
733 Ampure XP reagent. GEX adaptors were ligated, followed by Ampure XP cleanup. GEX
734 sample index PCR was followed by double-sided size selection using Ampure XP
735 reagent. GEX post-library construction quality was checked using the fragment analyzer,
736 and the library was sent for sequencing.

737 **Single cell RNAseq analysis**

738 Using Cellranger (Ver: 7.1.0), the fastq files were aligned to the mouse reference genome,
739 and feature counts were generated. Seurat (4.0) package was used to generate clusters

740 and analyze the data. Cells passing the following QC parameters were retained for
741 analysis (nCount_RNA>1000, nFeature_RNA > 500, singlets identified by Doublet
742 finder). A total of 38922 cells were included in the analysis. SCTransform with option
743 var.to.regress set to MitoPercent was used for data normalization. This was followed by
744 RunPCA, FindNeighbours, FindClusters, and RunUMAP. For plotting the functions in
745 Seurat, scCustomize, and custom codes were used. The cell types were identified
746 manually by marker gene expression, as described in the results section. Individual cell
747 types were subsetted and reclustered using the above-indicated commands. For
748 regulome analysis, SCENIC package was used. The codes for analysis will be made
749 available upon request.

750 **Cecal DNA isolation and 16S rRNA gene sequencing on the MinION™ platform**

751 We euthanized the mice and isolated the cecal matter from RCD, MBD, MFD, HFD and
752 RCD-MFD fed groups. We pooled ~ 200 mg of cecal matter from three mice as one
753 sample, in total each group has 6 samples. Total DNA was extracted by using (Bag, Saha
754 et al. 2016) method (a combinatorial method consisting of enzymatic, chemical and
755 mechanical lysis for proper lysis of microbial content).

756 The full-length 16S rRNA gene was amplified by using the barcoded primers provided by
757 16S barcoding kit 1-24 (SQK-16S024, Oxford-Nanopore Technologies). Amplification
758 was performed with the following PCR conditions: initial denaturation at 95 °C for 1 min,
759 25 cycles of 95 °C for 20 s, 55 °C for 30 s, and 65°C for 2 min, followed by a final extension
760 at 65 °C for 2 min. The amplified products were purified using AMPure® XP beads and
761 quantified using Qubit™ dsDNA HS and BR Assay Kits (Thermo Scientific, Catalog

762 number: Q32854). A total of 100 ng of DNA was incubated with 1 µl of Rapid Adapter at
763 room temperature for 5 min. The prepared DNA library (11 µl) was mixed with 34 µl of
764 Sequencing Buffer, 25.5 µl of Loading Beads, and 4.5 µl of water, loaded onto the (FLO-
765 MIN106; Oxford Nanopore Technologies), and sequenced on the MinION™. MINKNOW
766 software ver. 1.11.5 (Oxford Nanopore Technologies) was used for data acquisition.
767 Guppy basecaller (Oxford Nanopore Technologies) was used for base calling the
768 MinION™ sequencing data (FAST5 files) to generate pass reads (FASTQ format) with a
769 mean quality score > 7. The fastq files were aligned to the NCBI 16S rRNA dataset using
770 EPI2ME tools. Abundances were generated based on barcodes, and using microeco (R
771 Package), relative abundance, Alpha and beta diversity were calculated.

772 **Quantification of fecal SCFA using GC-MS.**

773 50 mg of caecal matter along with internal standard ribitol were mixed with 500ul of GC-
774 MS grade water followed by centrifugation. 10 μl of concentrated sulfuric acid (H_2SO_4)
775 was mixed in the 100ul of extract. 400 μl of diethyl ether (DE) is added to form liquid-
776 liquid extraction. 100 μl of DE extract is added into a GC vial. 1μl of BSTFA is added and
777 vortexed for 5 seconds followed by derivatization at 37 °C for 2 hours. 1ul of derivatized
778 samples were loaded to GC/MS (Agilent 7890A) coupled with 5975C MSD with Triple-
779 Axis Detector (TAD)). The injector, ion source, quadrupole, and the GC/MS interface
780 temperature were 260, 230, 150,and 280 °C, respectively. The flow rate of helium carrier
781 gas was kept at 1 ml/min. 1µl of the derivatized sample was injected with a 3 min of
782 solvent delay time and split ratio of 10:1. The initial column temperature was 40 °C and
783 held for 2 min, ramped to 150 °C at the rate of 15 °C/min and held for 1 min, and then

784 finally increased to 300 °C at the rate of 30°C/min and kept at this temperature for 5 min.
785 The ionization was carried out in the electron impact (EI) mode at 70 eV. The MS data
786 were acquired in full scan mode from m/z 30–400 with an acquisition frequency of 12.8
787 scans per second. The identification of compounds was confirmed by injection of pure
788 standards and comparison of the retention time and corresponding MS spectra.

789 **Conflict of Interest**

790 Authors declare no conflict of interest

791 **Ethical Standards Statement**

792 The authors of this manuscript certify that all experiments in the study were approved by
793 the Institutional Animal Ethics Committee.

794 **Acknowledgments**

795 We are grateful to Mr. Khem Singh Negi for genotyping mice and other technical help and
796 to Mr. B. N. Roy for help with histopathology experiments. We thank Dr. Nagarajan for his
797 help with animal experiments. We thank Dr. Ranjan Nanda for discussions on GC-MS
798 analysis. We thank Mr. Somdeb Chattopadhyay for running the SCENIC script and
799 providing the results.

800 **Funding**

801 The authors thank DBT, Government of India (BT/PR45456/PFN/20/1596/2022) for
802 G.A.A; and the National Institute of Immunology for research funding and fellowship for
803 CC, TB, NK.

804

805

806

807 **REFERENCES**

808 Aguilera, C., K. Nakagawa, R. Sancho, A. Chakraborty, B. Hendrich and A. Behrens (2011). "c-
809 Jun N-terminal phosphorylation antagonises recruitment of the Mbd3/NuRD repressor complex."
810 Nature **469**(7329): 231-235.

811 Al Nabhani, Z., S. Dulauroy, R. Marques, C. Cousu, S. Al Bounny, F. Dejardin, T. Sparwasser, M.
812 Berard, N. Cerf-Bensussan and G. Eberl (2019). "A Weaning Reaction to Microbiota Is Required
813 for Resistance to Immunopathologies in the Adult." Immunity **50**(5): 1276-1288 e1275.

814 Bag, S., B. Saha, O. Mehta, D. Anbumani, N. Kumar, M. Dayal, A. Pant, P. Kumar, S. Saxena, K.
815 H. Allin, T. Hansen, M. Arumugam, H. Vestergaard, O. Pedersen, V. Pereira, P. Abraham, R.
816 Tripathi, N. Wadhwa, S. Bhatnagar, V. G. Prakash, V. Radha, R. M. Anjana, V. Mohan, K. Takeda,
817 T. Kurakawa, G. B. Nair and B. Das (2016). "An Improved Method for High Quality
818 Metagenomics DNA Extraction from Human and Environmental Samples." Sci Rep **6**: 26775.

819 Ballard, O. and A. L. Morrow (2013). "Human milk composition: nutrients and bioactive factors."
820 Pediatr Clin North Am **60**(1): 49-74.

821 Barman, M., M. Gio-Batta, L. Andrieux, M. Stravik, R. Saalman, R. Fristedt, H. Rabe, A. Sandin,
822 A. E. Wold and A. S. Sandberg (2024). "Short-chain fatty acids (SCFA) in infants' plasma and
823 corresponding mother's milk and plasma in relation to subsequent sensitisation and atopic disease."
824 EBioMedicine **101**: 104999.

825 Barratt, M. J., S. Nuzhat, K. Ahsan, S. A. Frese, A. A. Arzamasov, S. A. Sarker, M. M. Islam, P.
826 Palit, M. R. Islam, M. C. Hibberd, S. Nakshatri, C. A. Cowardin, J. L. Guruge, A. E. Byrne, S.
827 Venkatesh, V. Sundaresan, B. Henrick, R. M. Duar, R. D. Mitchell, G. Casaburi, J. Prambs, R.
828 Flannery, M. Mahfuz, D. A. Rodionov, A. L. Osterman, D. Kyle, T. Ahmed and J. I. Gordon (2022).
829 "Bifidobacterium infantis treatment promotes weight gain in Bangladeshi infants with severe acute
830 malnutrition." Sci Transl Med **14**(640): eabk1107.

831 Blanton, L. V., M. R. Charbonneau, T. Salih, M. J. Barratt, S. Venkatesh, O. Ilkaveya, S.
832 Subramanian, M. J. Manary, I. Trehan, J. M. Jorgensen, Y.-m. Fan, B. Henrissat, S. A. Leyn, D. A.
833 Rodionov, A. L. Osterman, K. M. Maleta, C. B. Newgard, P. Ashorn, K. G. Dewey and J. I. Gordon
834 (2016). "Gut bacteria that prevent growth impairments transmitted by microbiota from
835 malnourished children." Science **351**(6275).

836 Butler, M. I., T. F. S. Bastiaanssen, C. Long-Smith, K. Berding, S. Morkl, A. M. Cusack, C. Strain,
837 K. Busca, P. Porteous-Allen, M. J. Claesson, C. Stanton, J. F. Cryan, D. Allen and T. G. Dinan
838 (2020). "Recipe for a Healthy Gut: Intake of Unpasteurised Milk Is Associated with Increased
839 Lactobacillus Abundance in the Human Gut Microbiome." Nutrients **12**(5).

840 Cani, P. D., J. Amar, M. A. Iglesias, M. Poggi, C. Knauf, D. Bastelica, A. M. Neyrinck, F. Fava,
841 K. M. Tuohy, C. Chabo, A. Waget, E. Delmee, B. Cousin, T. Sulpice, B. Chamontin, J. Ferrieres,
842 J. F. Tanti, G. R. Gibson, L. Casteilla, N. M. Delzenne, M. C. Alessi and R. Burcelin (2007).
843 "Metabolic endotoxemia initiates obesity and insulin resistance." Diabetes **56**(7): 1761-1772.

844 Canovas, B. and A. R. Nebreda (2021). "Diversity and versatility of p38 kinase signalling in health
845 and disease." Nature Reviews Molecular Cell Biology **22**(5): 346-366.

Cattin, A. L., J. Le Beyec, F. Barreau, S. Saint-Just, A. Houllier, F. J. Gonzalez, S. Robine, M. Pincon-Raymond, P. Cardot, M. Lacasa and A. Ribeiro (2009). "Hepatocyte nuclear factor 4alpha, a key factor for homeostasis, cell architecture, and barrier function of the adult intestinal epithelium." Mol Cell Biol **29**(23): 6294-6308.

Chawla, M., T. Mukherjee, A. Deka, B. Chatterjee, U. A. Sarkar, A. K. Singh, S. Kedia, J. Lum, M. K. Dhillon, B. Banoth, S. K. Biswas, V. Ahuja and S. Basak (2021). "An epithelial Nfkb2 pathway exacerbates intestinal inflammation by supplementing latent RelA dimers to the canonical NF-kappaB module." Proc Natl Acad Sci U S A **118**(25).

Chen, L., S. Wang, Y. Zhou, X. Wu, I. Entin, J. Epstein, S. Yaccoby, W. Xiong, B. Barlogie, J. D. Shaughnessy, Jr. and F. Zhan (2010). "Identification of early growth response protein 1 (EGR-1) as a novel target for JUN-induced apoptosis in multiple myeloma." Blood **115**(1): 61-70.

Chen, R. Y., I. Mostafa, M. C. Hibberd, S. Das, M. Mahfuz, N. N. Naila, M. M. Islam, S. Huq, M. A. Alam, M. U. Zaman, A. S. Raman, D. Webber, C. Zhou, V. Sundaresan, K. Ahsan, M. F. Meier, M. J. Barratt, T. Ahmed and J. I. Gordon (2021). "A Microbiota-Directed Food Intervention for Undernourished Children." N Engl J Med **384**(16): 1517-1528.

Coskun, M., J. T. Troelsen and O. H. Nielsen (2011). "The role of CDX2 in intestinal homeostasis and inflammation." Biochim Biophys Acta **1812**(3): 283-289.

Das, A., S. D. Gopinath and G. A. Arimbasseri (2022). "Systemic ablation of vitamin D receptor leads to skeletal muscle glycogen storage disorder in mice." Journal of Cachexia, Sarcopenia and Muscle **13**(1): 467-480.

Das, A., N. Jawla, V. Meena, S. D. Gopinath and G. A. Arimbasseri (2023). "Lack of vitamin D signalling shifts skeletal muscles towards oxidative metabolism." J Cachexia Sarcopenia Muscle.

Deleu, S., K. Arnauts, L. Deprez, K. Machiels, M. Ferrante, G. R. B. Huys, J. M. Thevelein, J. Raes and S. Vermeire (2023). "High Acetate Concentration Protects Intestinal Barrier and Exerts Anti-Inflammatory Effects in Organoid-Derived Epithelial Monolayer Cultures from Patients with Ulcerative Colitis." Int J Mol Sci **24**(1).

Dou, W., S. Mukherjee, H. Li, M. Venkatesh, H. Wang, S. Kortagere, A. Peleg, S. S. Chilimuri, Z. T. Wang, Y. Feng, E. R. Fearon and S. Mani (2012). "Alleviation of gut inflammation by Cdx2/Pxr pathway in a mouse model of chemical colitis." PLoS One **7**(7): e36075.

Duan, Y., L. Zeng, C. Zheng, B. Song, F. Li, X. Kong and K. Xu (2018). "Inflammatory Links Between High Fat Diets and Diseases." Front Immunol **9**: 2649.

El Abbas, S., C. Radermecker, Q. Bai, C. Beguin, J. Schyns, M. Meunier, D. Pirottin, C. J. Desmet, M. A. Meuwis, T. Art, E. Louis, S. Y. Tam, M. Tsai, F. Bureau, S. J. Galli and T. Marichal (2020). "Epithelial RABGEF1 deficiency promotes intestinal inflammation by dysregulating intrinsic MYD88-dependent innate signaling." Mucosal Immunol **13**(1): 96-109.

Ferré, P., J. F. Decaux, T. Issad and J. Girard (1986). "Changes in energy metabolism during the suckling and weaning period in the newborn." Reproduction Nutrition Développement **26**(2B): 619-631.

Hayakawa, Y., N. D. Huntington, S. L. Nutt and M. J. Smyth (2006). "Functional subsets of mouse natural killer cells." Immunol Rev **214**: 47-55.

Hayakawa, Y. and M. J. Smyth (2006). "CD27 dissects mature NK cells into two subsets with distinct responsiveness and migratory capacity." J Immunol **176**(3): 1517-1524.

Hildebrandt, M. A., C. Hoffmann, S. A. Sherrill-Mix, S. A. Keilbaugh, M. Hamady, Y. Y. Chen, R. Knight, R. S. Ahima, F. Bushman and G. D. Wu (2009). "High-fat diet determines the composition of the murine gut microbiome independently of obesity." Gastroenterology **137**(5): 1716-1724 e1711-1712.

Hsu, C. C., R. Okumura, D. Motooka, R. Sasaki, S. Nakamura, T. Iida and K. Takeda (2021). "Alleviation of colonic inflammation by Lypd8 in a mouse model of inflammatory bowel disease." Int Immunol **33**(7): 359-372.

Jaafar, R., S. Tran, A. N. Shah, G. Sun, M. Valdearcos, P. Marchetti, M. Masini, A. Swisa, S. Giacometti, E. Bernal-Mizrachi, A. Matveyenko, M. Hebrok, Y. Dor, G. A. Rutter, S. K. Koliwad and A. Bhushan (2019). "mTORC1-to-AMPK switching underlies β cell metabolic plasticity during maturation and diabetes." Journal of Clinical Investigation **129**(10): 4124-4137.

Jung, D., D. J. Mangelsdorf and U. A. Meyer (2006). "Pregnane X receptor is a target of farnesoid X receptor." J Biol Chem **281**(28): 19081-19091.

Kalhan, S. and P. Parimi (2000). "Gluconeogenesis in the fetus and neonate." Semin Perinatol **24**(2): 94-106.

Kempinski, R., D. Arabasz and K. Neubauer (2024). "Effects of Milk and Dairy on the Risk and Course of Inflammatory Bowel Disease versus Patients' Dietary Beliefs and Practices: A Systematic Review." Nutrients **16**(15).

Krueger, F., Z. Madeja, M. Hemberger, M. McMahon, S. J. Cook and S. J. Gaunt (2009). "Down-regulation of Cdx2 in colorectal carcinoma cells by the Raf-MEK-ERK 1/2 pathway." Cell Signal **21**(12): 1846-1856.

Laffin, M., R. Fedorak, A. Zalasky, H. Park, A. Gill, A. Agrawal, A. Keshteli, N. Hotte and K. L. Madsen (2019). "A high-sugar diet rapidly enhances susceptibility to colitis via depletion of luminal short-chain fatty acids in mice." Sci Rep **9**(1): 12294.

Lewis, K., F. Lutgendorff, V. Phan, J. D. Soderholm, P. M. Sherman and D. M. McKay (2010). "Enhanced translocation of bacteria across metabolically stressed epithelia is reduced by butyrate." Inflamm Bowel Dis **16**(7): 1138-1148.

Liu, Y. Y. (2023). "Controlling the human microbiome." Cell Syst **14**(2): 135-159.

Mandic, A. D., E. Bennek, J. Verdier, K. Zhang, S. Roubrocks, R. J. Davis, B. Denecke, N. Gassler, K. Streetz, A. Kel, M. Hornef, F. J. Cubero, C. Trautwein and G. Sellge (2017). "c-Jun N-terminal kinase 2 promotes enterocyte survival and goblet cell differentiation in the inflamed intestine." Mucosal Immunol **10**(5): 1211-1223.

Meijssen, M. A., S. L. Brandwein, H. C. Reinecker, A. K. Bhan and D. K. Podolsky (1998). "Alteration of gene expression by intestinal epithelial cells precedes colitis in interleukin-2-deficient mice." Am J Physiol **274**(3): G472-479.

Modica, S., M. Cariello, A. Morgano, I. Gross, M. C. Vegliante, S. Murzilli, L. Salvatore, J. N. Freund, C. Sabba and A. Moschetta (2014). "Transcriptional regulation of the intestinal nuclear bile acid farnesoid X receptor (FXR) by the caudal-related homeobox 2 (CDX2)." J Biol Chem **289**(41): 28421-28432.

Mostafa, I., M. C. Hibberd, S. J. Hartman, M. H. Hafizur Rahman, M. Mahfuz, S. M. T. Hasan, P. Ashorn, M. J. Barratt, T. Ahmed and J. I. Gordon (2024). "A microbiota-directed complementary food intervention in 12-18-month-old Bangladeshi children improves linear growth." EBioMedicine **104**: 105166.

Narula, N., E. C. L. Wong, M. Dehghan, A. Mente, S. Rangarajan, F. Lanas, P. Lopez-Jaramillo, P. Rohatgi, P. V. M. Lakshmi, R. P. Varma, A. Orlandini, A. Avezum, A. Wielgosz, P. Poirier, M. A. Almadi, Y. Altuntas, K. K. Ng, J. Chifamba, K. Yeates, T. Puoane, R. Khatib, R. Yusuf, K. B. Bostrom, K. Zatonska, R. Iqbal, L. Weida, Z. Yibing, L. Sidong, A. Dans, A. Yusufali, N. Mohammadifard, J. K. Marshall, P. Moayyedi, W. Reinisch and S. Yusuf (2021). "Association of ultra-processed food intake with risk of inflammatory bowel disease: prospective cohort study." BMJ **374**: n1554.

Okumura, R., T. Kurakawa, T. Nakano, H. Kayama, M. Kinoshita, D. Motooka, K. Gotoh, T. Kimura, N. Kamiyama, T. Kusu, Y. Ueda, H. Wu, H. Iijima, S. Barman, H. Osawa, H. Matsuno, J. Nishimura, Y. Ohba, S. Nakamura, T. Iida, M. Yamamoto, E. Umemoto, K. Sano and K. Takeda (2016). "Lypd8 promotes the segregation of flagellated microbiota and colonic epithelia." Nature **532**(7597): 117-121.

Opstelten, J. L., M. Leenders, V. K. Dik, S. S. Chan, F. D. van Schaik, K. T. Khaw, R. Luben, G. Hallmans, P. Karling, S. Lindgren, O. Grip, T. J. Key, F. L. Crowe, H. Boeing, M. M. Bergmann, K. Overvad, D. Palli, G. Masala, A. Racine, F. Carbonnel, M. C. Boutron-Ruault, A. Tjonneland, A. Olsen, V. Andersen, R. Kaaks, V. A. Katzke, R. Tumino, A. Trichopoulou, P. D. Siersema, H. B. Bueno-de-Mesquita, A. R. Hart and B. Oldenburg (2016). "Dairy Products, Dietary Calcium, and Risk of Inflammatory Bowel Disease: Results From a European Prospective Cohort Investigation." Inflamm Bowel Dis **22**(6): 1403-1411.

Paredes, A., R. Justo-Mendez, D. Jimenez-Blasco, V. Nunez, I. Calero, M. Villalba-Orero, A. Alegre-Marti, T. Fischer, A. Gradillas, V. A. R. Sant'Anna, F. Were, Z. Huang, P. Hernansanz-Agustin, C. Contreras, F. Martinez, E. Camafeita, J. Vazquez, J. Ruiz-Cabello, E. Area-Gomez, F. Sanchez-Cabo, E. Treuter, J. P. Bolanos, E. Estebanez-Perpina, F. J. Ruperez, C. Barbas, J. A. Enriquez and M. Ricote (2023). "gamma-Linolenic acid in maternal milk drives cardiac metabolic maturation." Nature **618**(7964): 365-373.

Parhar, K., A. Ray, U. Steinbrecher, C. Nelson and B. Salh (2003). "The p38 mitogen-activated protein kinase regulates interleukin-1beta-induced IL-8 expression via an effect on the IL-8 promoter in intestinal epithelial cells." Immunology **108**(4): 502-512.

Peng, Y., Y. Fang, Z. Li, C. Liu and W. Zhang (2024). "Saa3 promotes pro-inflammatory macrophage differentiation and contributes to sepsis-induced AKI." Int Immunopharmacol **127**: 111417.

Perler, B. K., E. S. Friedman and G. D. Wu (2023). "The Role of the Gut Microbiota in the Relationship Between Diet and Human Health." Annu Rev Physiol **85**: 449-468.

Roy, P. K., F. Rashid, J. Bragg and J. A. Ibdah (2008). "Role of the JNK signal transduction pathway in inflammatory bowel disease." World J Gastroenterol **14**(2): 200-202.

Samak, G., T. Suzuki, A. Bhargava and R. K. Rao (2010). "c-Jun NH2-terminal kinase-2 mediates osmotic stress-induced tight junction disruption in the intestinal epithelium." Am J Physiol Gastrointest Liver Physiol **299**(3): G572-584.

Sancho, R., A. S. Nateri, A. G. de Vinuesa, C. Aguilera, E. Nye, B. Spencer-Dene and A. Behrens (2009). "JNK signalling modulates intestinal homeostasis and tumourigenesis in mice." EMBO J **28**(13): 1843-1854.

Shindo, R., T. Katagiri, S. Komazawa-Sakon, M. Ohmuraya, W. Takeda, Y. Nakagawa, N. Nakagata, T. Sakuma, T. Yamamoto, C. Nishiyama, T. Nishina, S. Yamazaki, H. Kameda and H. Nakano (2020). "Regenerating islet-derived protein (Reg)3beta plays a crucial role in attenuation of ileitis and colitis in mice." Biochem Biophys Rep **21**: 100738.

Shuai, M., L. S. Zuo, Z. Miao, W. Gou, F. Xu, Z. Jiang, C. W. Ling, Y. Fu, F. Xiong, Y. M. Chen and J. S. Zheng (2021). "Multi-omics analyses reveal relationships among dairy consumption, gut microbiota and cardiometabolic health." EBioMedicine **66**: 103284.

Song, Y., S. Kato and J. C. Fleet (2003). "Vitamin D Receptor (VDR) Knockout Mice Reveal VDR-Independent Regulation of Intestinal Calcium Absorption and ECaC2 and Calbindin D9k mRNA." The Journal of Nutrition **133**(2): 374-380.

Stolovich-Rain, M., J. Enk, J. Vikesa, F. C. Nielsen, A. Saada, B. Glaser and Y. Dor (2015). "Weaning triggers a maturation step of pancreatic beta cells." Dev Cell **32**(5): 535-545.

Suriano, F., S. Vieira-Silva, G. Falony, A. de Wouters d'Oplinter, P. Paone, N. M. Delzenne, A. Everard, J. Raes, M. Van Hul and P. D. Cani (2023). "Fat and not sugar as the determining factor for gut microbiota changes, obesity, and related metabolic disorders in mice." Am J Physiol Endocrinol Metab **324**(1): E85-E96.

Ulven, S. M., K. B. Holven, A. Gil and O. D. Rangel-Huerta (2019). "Milk and Dairy Product Consumption and Inflammatory Biomarkers: An Updated Systematic Review of Randomized Clinical Trials." Adv Nutr **10**(suppl_2): S239-S250.

Van de Sande, B., C. Flerin, K. Davie, M. De Waegeneer, G. Hulselmans, S. Aibar, R. Seurinck, W. Saelens, R. Cannoodt, Q. Rouchon, T. Verbeiren, D. De Maeyer, J. Reumers, Y. Saeys and S. Aerts (2020). "A scalable SCENIC workflow for single-cell gene regulatory network analysis." Nat Protoc **15**(7): 2247-2276.

Vemuri, K., S. H. Radi, F. M. Sladek and M. P. Verzi (2023). "Multiple roles and regulatory mechanisms of the transcription factor HNF4 in the intestine." Front Endocrinol (Lausanne) **14**: 1232569.

Wang, L., D. E. Fouts, P. Starkel, P. Hartmann, P. Chen, C. Llorente, J. DePew, K. Moncera, S. B. Ho, D. A. Brenner, L. V. Hooper and B. Schnabl (2016). "Intestinal REG3 Lectins Protect against Alcoholic Steatohepatitis by Reducing Mucosa-Associated Microbiota and Preventing Bacterial Translocation." Cell Host Microbe **19**(2): 227-239.

Wang, P. Y., S. R. Wang, L. Xiao, J. Chen, J. Y. Wang and J. N. Rao (2017). "c-Jun enhances intestinal epithelial restitution after wounding by increasing phospholipase C-gamma1 transcription." Am J Physiol Cell Physiol **312**(4): C367-C375.

Wang, Y., Y. Yu, L. Li, M. Zheng, J. Zhou, H. Gong, B. Feng, X. Wang, X. Meng, Y. Cui, Y. Xia, S. Chu, L. Lin, H. Chang, R. Zhou, M. Ma, Z. Li, R. Ji, M. Lu, X. Yang, X. Zuo, S. Li and Y. Li (2023). "Bile acid-dependent transcription factors and chromatin accessibility determine regional heterogeneity of intestinal antimicrobial peptides." Nat Commun **14**(1): 5093.

Waterhouse, C. C. and A. W. Stadnyk (1999). "Rapid expression of IL-1beta by intestinal epithelial cells in vitro." Cell Immunol **193**(1): 1-8.

Wilde, J., E. Slack and K. R. Foster (2024). "Host control of the microbiome: Mechanisms, evolution, and disease." Science **385**(6706): eadi3338.

Wu, X., F. Wang, M. Chen, Y. Qi, L. Song, N. Zheng, J. Wang and Y. Zhang (2024). "A comprehensive study of the whole profiles of short-chain fatty acids in milk." J Dairy Sci.

Xu, D., S. Zhou, Y. Liu, A. L. Scott, J. Yang and F. Wan (2024). "Complement in breast milk modifies offspring gut microbiota to promote infant health." Cell **187**(3): 750-763 e720.

Yu, J., K. Yang, J. Zheng, P. Zhao, J. Xia, X. Sun and W. Zhao (2022). "Activation of FXR and inhibition of EZH2 synergistically inhibit colorectal cancer through cooperatively accelerating FXR nuclear location and upregulating CDX2 expression." Cell Death Dis **13**(4): 388.

Zhang, P., S. M. Pronovost, M. Marchetti, C. Zhang, X. Kang, T. Kandelouei, C. Li and B. A. Edgar (2024). "Inter-cell type interactions that control JNK signaling in the Drosophila intestine." Nature Communications **15**(1).

Zhang, Y., S. Tu, X. Ji, J. Wu, J. Meng, J. Gao, X. Shao, S. Shi, G. Wang, J. Qiu, Z. Zhang, C. Hua, Z. Zhang, S. Chen, L. Zhang and S. J. Zhu (2024). "Dubosiella newyorkensis modulates immune tolerance in colitis via the L-lysine-activated AhR-IDO1-Kyn pathway." Nat Commun **15**(1): 1333.

Zhang, Y., L. Yin, J. Anderson, H. Ma, F. J. Gonzalez, T. M. Willson and P. A. Edwards (2010). "Identification of novel pathways that control farnesoid X receptor-mediated hypocholesterolemia." J Biol Chem **285**(5): 3035-3043.

Zhao, X. H., P. Zhao, Z. Deng, T. Yang, Y. X. Qi, L. Y. An, D. L. Sun and H. Y. He (2023). "Integrative analysis reveals marker genes for intestinal mucosa barrier repairing in clinical patients." iScience **26**(6): 106831.

Zheng, W., X. Wang, J. Liu, X. Yu, L. Li, H. Wang, J. Yu, X. Pei, C. Li, Z. Wang, M. Zhang, X. Zeng, F. Zhang, C. Wang, H. Chen and H. Z. Chen (2022). "Single-cell analyses highlight the proinflammatory contribution of C1q-high monocytes to Behcet's disease." Proc Natl Acad Sci U S A **119**(26): e2204289119.

1039 **FIGURE TITLES AND LEGENDS:**

1040 **Figure 1**: **Post-weaning milk-based diets protect from DSS-induced gut**
1041 **inflammation.**

1042 **A**: An Illustration of the DSS-induced mouse colitis experimental model. 3 weeks old mice
1043 were weaned to the indicated diets. After 4 weeks, they were subjected to 1.5% DSS
1044 treatment.

1045 **B**: Disease severity score calculated from the rectal bleeding and stool consistency for
1046 different experimental groups indicated.

1047 **C**: Percentage of body weight after DSS treatment with day 0 as the baseline. Different
1048 experimental groups are indicated.

1049 **D**: Colon length measured in centimeters for different experimental groups. The images
1050 of the colon are given in Figure S1B.

1051 **E**: Representative images of H&E-stained colon tissue sections (DSS- or water-treated
1052 mice fed RCD, MBD, MFD, and HFD. Scale bars are shown (100 px).

1053 **F-H**: mRNA levels of Proinflammatory cytokines IL1β, IL6, and TNFα analyzed by RT-
1054 qPCR, with Ct values normalized to *Actb* mRNA, in colon tissues of mice fed on RCD,
1055 MBD, MFD, and HFD after 7 days of DSS- or water-treatment.

1056 Data are mean ± SEM, with statistical analysis by two-way ANOVA with Tukey's multiple
1057 comparison test (B, C, D, F, G and H). *$p < 0.05$, **$p < 0.01$, ***$p < 0.005$, ****$p < 0.001$

1058 **Figure 2: MBD-fed mice exhibit reduced Immune activation after DSS treatment.**

1059 **A**: UMAP and donut plots showing the distribution of B cells from different experimental
1060 groups across different clusters. The experimental groups are RCD-H2O (RCD on water),
1061 RCD-DSS (RCD on 1.5% DSS), MBD-H2O (MBD on water), and MBD-DSS (MBD on
1062 1.5% DSS). B cells were identified based on markers *Cd79a*, *Ms4a1*, and *Cd19*. The
1063 percentage of cells belonging to some of the clusters is shown next to each donut plot.

1064 **B**: Violin plot for average expression of *Igha, Ighd,* and *Ighm* across the B cell clusters to
1065 show naive, plasma, and class-switched B cells. cell types are color coded on the X axis.

1066 **C**: Violin plot for average gene expression for *Cd80* and *Cd44*, markers for activated B
1067 cells.

1068 **D**: UMAP plots colored by the expression of T cell marker genes (*Cd4, Cd8a, Cd8b1,*
1069 *Ifng, Gzma,* and *Cd69)*. The intensity of the color indicates the expression levels as shown
1070 in the color scale given with each plot.

1071 **E**: Dot plot showing expression of various T cell markers, highlighting different subsets
1072 such as Treg, Th1, Th2, and Th17 cells. The color indicates the expression level and the
1073 size of the dots indicates the percentage of cells expressing the gene.

1074 **F**: The percentage of cells from each experimental group falling into different clusters was
1075 plotted as a stacked bar plot. Each bar is standardized to have the same height by using
1076 the position_fill() argument in ggplot2. Dark blue represents RCD-H2O, green represents
1077 RCD-DSS, violet represents MBD-H2O, and orange represents MBD-DSS.

1078 **G**: UMAP representation of all myeloid cells (*Cd14*, *Itgam*, *Fcgr3*, *Itgax)* showing 22
1079 clusters

1080 **H**: Donut plots show the distribution of myeloid cells from different experimental groups
1081 across different clusters. The percentage of cells belonging to some of the clusters is
1082 shown next to each donut plot.

1083 **I**: UMAP plots colored by the expression of cytotoxic NK cell marker genes (*Klrk1/NKG2D,*
1084 *Cd7, Cd27, Gzma, Gzmb, Prf1, Fasl,* and *Tnfsf10*). The intensity of the color indicates
1085 the expression levels as shown in the color scale given with each plot.

1086 **J**: Dot plot showing expression of various macrophage and inflammatory monocyte
1087 marker genes. The color indicates the expression level, and the size of the dots indicates
1088 the percentage of cells expressing the gene.

1089

1090 **Figure 3**: **Milk-based diets maintain gut barrier function even after DSS treatment.**
1091 **A**: UMAP and donut plots showing the distribution of epithelial cells from different
1092 experimental groups across different clusters. The experimental groups are RCD-H2O
1093 (RCD on water), RCD-DSS (RCD on 1.5% DSS), MBD-H2O (MBD on water), and MBD-
1094 DSS (MBD on 1.5% DSS). The percentage of cells belonging to indicated clusters is
1095 shown next to each donut plot.

1096 **B**: UMAP and donut plots showing the distribution of epithelial cells from different
1097 experimental groups across different cell types.

1098 **C&D**: Violin plot showing module scores for inflammatory and gut barrier repair
1099 associated gene sets across all clusters (Supplementary Table 2).

1100 **E**: Dot plot showing expression of gut barrier-associated genes across clusters. The color
1101 indicates the expression level, and the size of the dots indicates the percentage of cells
1102 expressing the gene.

1103 **F-H**: Expression of gut barrier-associated genes *Ocln* (F)*, Cld7* (G), and *Tjp1* (H) analyzed
1104 by RT-qPCR, with Ct values normalized to *Actb*, in colon tissues of DSS- or water-treated
1105 mice fed RCD, MBD, MFD, and HFD.

1106 **I&J**: Expression levels of transcription factor genes, *Cdx2* (I) and *Hnf4a* (J)*,* analyzed by
1107 RT-qPCR. Ct values were normalized to *Actb*, in colon tissues of DSS- or water-treated
1108 mice fed RCD, MBD, MFD, and HFD.

1109 **K**: Gut permeability assay, measuring fluorescence in the serum of DSS- or water-treated
1110 mice fed RCD, MBD, MFD, and HFD 10 minutes after oral gavage of FITC-dextran.

1111 Data are mean ± SEM, with statistical analysis by two-way ANOVA with Tukey's multiple
1112 comparison test (E, F, G, H and I) and one-way ANOVA with Tukey's multiple comparison
1113 test (J). *$p < 0.05$, **$p < 0.01$, ***$p < 0.005$, ****$p < 0.001$.

1114 **Figure 4**: **Milk-based diets elicit protective effects against gut inflammation by**
1115 **activating the JNK2 pathway in the epithelial cells.**

1116 **A**: Heatmap showing the regulome expression calculated using the SCENIC package,
1117 highlighting transcription factors whose targets are enriched in clusters 2, 10, and 11.

1118 **B**: Dot plot showing expression levels of gut barrier-associated transcription factors
1119 identified in SCENIC analysis and enriched in clusters 2, 10, and 11.

1120 **C**: Dot plots of antimicrobial protein (AMPs) genes (*Reg3b, Reg3g, and Lypd8)* and
1121 associated transcription factors (*Vdr, Cdx2, Nr1h4*) across epithelial cell clusters,
1122 highlighting the enrichment of these genes in clusters 2, 10, and 11.

1123 **D&E**: Expression levels of AMP genes (*Lypd8* and *Reg3b)* analyzed by RT-qPCR, with
1124 Ct values normalized to *Actb*, in colon tissues of DSS- or water-treated mice fed RCD,
1125 MBD, MFD, and HFD.

1126 **F&G**: Western blot analysis of intestinal epithelial cells (IECs) isolated from colons of mice
1127 subjected to RCD, MBD, MFD, and HFD (without DSS treatment), probed with antibodies
1128 against p-JNK, JNK, p-p38, and p38. Representative blot (left panel) and densitometric
1129 quantification (right panel) are shown. In the JNK blot, the upper band (indicated by an
1130 asterisk) shows JNK2, while the lower band shows JNK1. In the P38 blot, the lower band
1131 (indicated by the arrowhead) indicates the P38; the upper band is a non-specific band.

1132 **H-J**: JNK inhibitor II or vehicle was administered to RCD and MFD-fed mice 24 hours
1133 before treatment with DSS. Disease severity score (H), body weight percentage (I), and
1134 total colon length (J) of DSS and water groups are plotted.

1135 **K-M**: mRNA levels of proinflammatory cytokines (*Tnfa* and *Il1b)* (K)*,* gut barrier genes
1136 (*Tjp1, Ocln,* and *Muc2)* (L)*, and* AMPs (*Lypd8* and *Reg3b)* (M), in the colon tissue of JNK
1137 inhibitor II treated mice were analyzed by RT-qPCR, with Ct values normalized against
1138 *Actb*. Dietary groups are indicated.

1139 (**N**): p-p38 and p38 levels were analyzed in IECs from mice fed on RCD and MFD, isolated
1140 7 days after p-JNK inhibition. Representative blot (left panel) and densitometric
1141 quantification (right panel) are shown.

1142 Data are mean ± SEM, with statistical analysis by two-way ANOVA with Tukey's multiple
1143 comparison test (D, E, H, I, J, K, L, and M) and one-way ANOVA with Tukey's multiple
1144 comparison test (F, G, and N). *$p < 0.05$, **$p < 0.01$, ***$p < 0.005$, ****$p < 0.001$.

1145

1146 **Figure 5**: **A break in the milk-based diet regimen alleviates JNK2 phosphorylation**
1147 **and protective effects.**

1148 **A**: Schematic illustration of repeated DSS exposure experimental workflow.

1149 **B**: Disease severity score of RCD(I&II) and MFD(I&II) groups during the first DSS
1150 challenge (DSS-I) and second DSS challenge (DSS-II).

1151 **C**: Daily body weight (as the percentage with the day 0 as 100%) of mice in RCD(I&II)
1152 and MFD(I&II) groups along with their control groups (without any DSS treatment). The
1153 dashed vertical lines demarcate the DSS treatment periods (DSS-1 and DSS-II).

1154 **D:** Colon lengths of mice in RCD(I&II) and MFD(I&II) groups, along with their control
1155 groups (without DSS treatment), were measured at the end of the experiment and plotted.

1156 **E**: Expression levels of proinflammatory cytokines (*Tnfa* and *Il1b*) were analyzed by RT-
1157 qPCR, with Ct values normalized to *Actb*, in colon tissues of repeated DSS exposure and
1158 control groups.

1159 **F-H**: Disease severity scores, body weight change, and total colon length of mice treated
1160 with 1.5% DSS and subjected to RCD, MFD, and RCD-MFD diets.

1161 **I**: Representative images of H&E stained colon tissues from DSS- or water-treated mice
1162 fed on RCD-MFD.

1163 **J**: Expression levels of proinflammatory cytokines (*Ifng, Tnfa* and *Il1b*) analyzed by RT-
1164 qPCR, with Ct values normalized to *Actb*, in colon tissues of DSS- or water-treated mice
1165 fed on RCD, MFD, and RCD-MFD.

1166 **K**&**L**: Expression levels of gut barrier genes (*Tjp1, Ocln, Cld7, and Muc2*) (K) and AMPs
1167 (*Reg3b,* and *Lypd8*) (L) analyzed by RT-qPCR, with Ct values normalized to *Actb*, in IECs
1168 of mice, fed RCD, MFD, HFD, and RCD-MFD.

1169 **M**&**N**: Western blot analysis of IECs isolated from mice fed on RCD, MFD, HFD, and
1170 RCD-MFD, showing p-JNK, JNK, p-p38, and p38.

1171 Data are mean ± SEM, with statistical analysis by two-way ANOVA with Tukey's multiple
1172 comparison test (B, C, D, E, F, G, H and J) and one-way ANOVA with Tukey's multiple
1173 comparison test (K, L, M, and N). *$p < 0.05$, **$p < 0.01$, ***$p < 0.005$, ****$p < 0.001$.

1174 **Figure 6: *Dubosiella Newyorkensis*, enriched in the milk-based diet groups,**
1175 **provides gut protection.**

1176 **A**: Schematic illustration of the experimental workflow for antibiotic treatment.

1177 **B**: Western blots of IECs isolated from mice with or without antibiotic (ABX) treatment,
1178 fed RCD, MFD, and HFD, showing levels of p-JNK and total JNK (left panel).
1179 Quantification of the blots is on the right panel.

1180 **C**&**D**: Expression levels of gut homeostasis genes *Hnf4a* (C)*, Reg3b,* and *Lypd8* (D)
1181 analyzed by RT-qPCR, with Ct values normalized to *Actb*, in IECs of mice treated with
1182 ABX, fed RCD, MFD, and HFD.

1183 **E**&**F**: Microbial-diversity indices [Shannon and inversed Simpson (E) and Chao index (F)]
1184 of fecal microbiome isolated from mice fed on RCD, MFD, HFD, and RCD-MFD.

1185 **G**: Stacked bar plot showing the abundance of the top 10 species across different
1186 experimental groups. *D. newyorkensis* is highlighted.

1187 **H**: Box plot showing higher levels of *D. newyorkensis* in the milk-based diet groups.

1188 **I-K**: Body weight, disease severity score, and colon length of control and *D.newyorkensis*
1189 treated mice challenged with DSS.

1190 **L-N**: Expression levels of proinflammatory cytokines (*Tnfa* and *Il1b*) (L), gut barrier genes
1191 (*Cld7, Tjp1,* and *Muc2*) (M) and AMPs (*Reg3b* and *Lypd8*) (N) analyzed by RT-qPCR,
1192 with Ct values normalized to *Actb*, in colon tissues of mice treated with *D. newyorkensis.*

1193 **O**: Western blot analyses of IECs isolated from mice treated with *D. newyorkensis*,
1194 showing p-JNK and total-JNK levels.

1195 Data are mean ± SEM, with statistical analysis by two-way ANOVA with Tukey's multiple
1196 comparison test (C, D, I, J, K, L, M and N) and one-way ANOVA with Tukey's multiple
1197 comparison test (B, E, H, and O). *$p < 0.05$, **$p < 0.01$, ***$p < 0.005$, ****$p < 0.001$.

1198

1199 **Figure 7: Acetate induces the JNK2 pathway in the colonic epithelium to enhance**
1200 **gut barrier function.**

1201 **A**: Quantification of fecal acetate, propionate, and butyrate using GC-MS in different
1202 experimental groups.

1203 **B**: Levels of acetate in the fecal matter of mice treated with *D. newyorkensis* and control
1204 mice.

1205 **C**-**E**: Disease severity score, body weight, and colon length of acetate and DSS-treated
1206 mice.

1207 **F**&**G**: RT-qPCR analysis of proinflammatory cytokines (*Tnfa, Il1b,* and *Ifng)* (F) and gut
1208 barrier genes *(Ocln, Muc2*, and *Hnf4a)* (G) in colon tissues of mice treated with *D.*
1209 *newyorkensis* with or without 1.5% DSS challenge.

1210 **H**: Representative images of H&E-stained colon tissue sections of control and acetate-
1211 treated mice with or without DSS insult.

1212 **I**: Western blot analyses of IECs isolated from control and acetate-treated mice showing
1213 p-JNK and total-JNK levels. Densitometric quantitation is given in the right panel.

1214 **J**: RT-qPCR analysis of antimicrobial protein mRNAs (*Reg3b* and *Lypd8*) in colon tissues
1215 of control or acetate-treated mice with or without 1.5% DSS challenge.

1216 Data are mean ± SEM, with statistical analysis by two-way ANOVA with Tukey's multiple
1217 comparison test (B, C, D, E, and F), one-way ANOVA with Tukey's multiple comparison
1218 test (A, H, and I). *$p < 0.05$, **$p < 0.01$, ***$p < 0.005$, ****$p < 0.001$.

1219

1220 **Figure S1: Post-weaning milk-based diets protect from DSS-induced gut**
1221 **inflammation.**

1222 **A**: Composition of macronutrients in different diets: RCD, MBD, MFD, and HFD.

1223 **B**: Representative images of the colon from DSS- or water-treated mice fed RCD, MBD,
1224 MFD, and HFD.

1225 **C&D**: Expression levels of anti-inflammatory cytokines IL10 and TGFβ analyzed by RT-
1226 qPCR, with Ct values normalized to *Actb* mRNA, in colon tissues of DSS- or water-treated
1227 mice fed on RCD, MBD, MFD, and HFD.

1228 Data are mean ± SEM, with statistical analysis by two-way ANOVA with Tukey's multiple
1229 comparison test (C, and D). *$p < 0.05$, **$p < 0.01$, ***$p < 0.005$, ****$p < 0.001$

1230

1231 **Figure S2: MBD-fed mice exhibit reduced Immune activation after DSS treatment.**

1232 **A**: Schematic illustration of the scRNAseq experimental workflow. 4 weeks after weaning
1233 onto MBD or RCD, mice were either subjected to water or 1.5% DSS for 7 days. Colon
1234 was dissected, and single-cell suspensions were made. IECs, myeloid cells, T cells, and
1235 B cells were isolated, pooled, and subjected to scRNAseq experiment.

1236 **B**: Gating strategy for sorting epithelial, T cell, B cell, and myeloid cells from colon.

1237 **C**: UMAP representation of all detected cells, highlighting epithelial cells, B cells, T cells,
1238 and myeloid cells based on markers.

1239 **D**: Dot plot of marker genes highlighting epithelial cells (*Epcam, Krt8,* and *Krt18*), B cells
1240 (*CD79a, Ms4a1,* and *CD19*), T cells (*CD3d, CD3e,* and *CD3g*), and myeloid cells (*CD14,*
1241 *Itgam, Fcgr3, Itgax, H2-Aa,* and *H2-Ab1*). The color indicates the expression level, and
1242 the size of the dots indicates the percentage of cells expressing the gene.

1243 **E**: UMAP representations and donut plots showing the distribution of B cells from different
1244 experimental groups across different cell types. The experimental groups are RCD-H2O
1245 (RCD on water), RCD-DSS (RCD on 1.5% DSS), MBD-H2O (MBD on water), and MBD-
1246 DSS (MBD on 1.5% DSS). The percentage of cells belonging to some of the cell types is
1247 shown next to each donut plot.

1248 **F**: UMAP representation and donut plot showing the distribution of T cells across different
1249 clusters. The percentage of cells belonging to some of the cell types is shown next to the
1250 donut plot.

1251 **G-I**: Dot plots showing expression levels of macrophage, cDC2, and monocyte marker
1252 genes. The color indicates the expression level, and the size of the dots indicates the
1253 percentage of cells expressing the gene.

1254 **J**: Bar plot showing -log10(adjusted p-value) of GO terms enriched in cluster 0 of myeloid
1255 cells. The color indicates the number of genes differentially expressed in cluster 0 that
1256 overlaps with the indicated GO term.

1257

1258 **Figure S3: - Milk-based diets maintain gut barrier function even after DSS**
1259 **treatment.**

1260 **A-G**: Dot plots showing expression levels of marker genes for stem cells (A), colonocytes
1261 (B), goblet cells (C), cycling TA (D), TA (E), tuft cells (F), and enteroendocrine cells (G)
1262 across all epithelial clusters, colored by average gene expression. Dot size indicate the
1263 percentage of cells expressing the gene.

1264 **H&J**: The percentage of cells from each experimental group falling into different clusters
1265 was plotted as a stacked bar plot. Each bar is standardized to have the same height using
1266 the position_fill() argument in ggplot2. Salmon represents RCD-H2O, green represents
1267 RCD-DSS, dark turquoise represents MBD-H2O, and violet represents MBD-DSS.

1268 **I**: Dot plots showing expression levels of inflammatory genes across epithelial cell
1269 clusters. Color intensity indicates the average expression level, and the size of the dot
1270 indicates the percentage of cells expressing the gene.

1271 **Figure S4: - Milk-based diets elicit protective effects against gut inflammation by**
1272 **activating the JNK2 pathway in the epithelial cells.**

1273 **A**: Heatmap showing the regulome expression calculated using the SCENIC package.

1274 **B**: Network graph showing the interaction between transcription factors identified in the
1275 SCENIC analysis and gut barrier and AMP genes analyzed by StringDB.

1276 **C&D**: p-p38 target genes associated with inflammation (*Cox2, and Ptges2)* analyzed by
1277 RT-qPCR, with Ct values normalized to *Actb*, in colon tissues of DSS- or water-treated
1278 mice, fed RCD, MBD, MFD, and HFD.

1279 **E**: Western blot analysis for p-JNK and JNK levels in IECs isolated from JNK inhibitor II
1280 treated mice fed on RCD. Samples were collected at 6 hrs and 24 hrs post inhibitor
1281 treatment.

1282 **F**: Representative images of colon tissues, DSS- or water-treated, with or without JNK
1283 inhibitor II. Diet groups are indicated.

1284 **G**: Representative images of H&E-stained colon tissue sections of RCD and MFD-fed
1285 mice treated with DSS- or water and subjected to JNK inhibition or vehicle treatment.

1286 **H**: Gut-barrier associated genes *Cld7 and Hnf4a* analyzed by RT-qPCR, with Ct values
1287 normalized to *Actb*, in colon tissues of DSS- or water-treated mice with or without JNK
1288 inhibition, fed on MFD.

1289 **I:** p-JNK and JNK levels were analyzed in IECs from mice fed on RCD and MFD, isolated
1290 7 days after p-JNK inhibition. Representative blot (left panel) and densitometric
1291 quantification (right panel) are shown.

1292 Data are mean ± SEM, with statistical analysis by two-way ANOVA with Tukey's multiple
1293 comparison test (C, D, and H) and one-way ANOVA with Tukey's multiple comparison
1294 test (I). *$p < 0.05$, **$p < 0.01$, ***$p < 0.005$, ****$p < 0.001$.

1295 **Figure S5: A break in the milk-based diet regimen alleviates JNK2 phosphorylation**
1296 **and protective effects.**

1297 **A**: Disease severity scores of RCD(I&II), MFD(I&II), and RCD(I)-MFD(II) groups of mice
1298 treated with 1.5% DSS, displaying scores from both rounds of the DSS insults (DSS-I &
1299 DSS-2).

1300 **B**: Daily body weight percentage (Day 0 as baseline) of RCD(I&II), MFD(I&II), and RCD(I)-
1301 MFD(II) groups of mice (control and treated with 1.5% DSS) over 28 days. The duration
1302 of each DSS treatment is demarcated by dashed vertical lines.

1303 **C**: Colon length of RCD(I&II), MFD(I&II), and RCD(I)-MFD(II) groups of mice treated with
1304 two rounds of DSS or water. Colon length was measured at the end of the experiment.

1305 **D**: Schematic illustration of the experimental workflow for data shown in Figures 5F-N).

1306 Data are mean ± SEM, with statistical analysis by two-way ANOVA with Tukey's multiple
1307 comparison test (A, B, and C). *$p < 0.05$, **$p < 0.01$, ***$p < 0.005$, ****$p < 0.001$.

1308

1309 **Figure S6: *Dubosiella Newyorkensis, enriched in the milk-based diet groups,***
1310 ***provides gut protection*.**

1311 **A**: LB agar plate showing fecal microbiota depletion in antibiotic-treated mice. 20 mg of
1312 fecal matter was resuspended in 1 ml PBS and diluted 1/4 fold and 1/8 fold and spotted
1313 on the plate. Each black circle represents sample from a mouse.

1314 **B**: Western blot analyses of IECs isolated from mice with or without antibiotic (ABX)
1315 treatment, fed RCD, MFD, and HFD, showing p-p38 and total p38. Panel on the right-
1316 hand side shows densitometric quantification.

1317 **C&D**: RT-qPCR analysis of expression of inflammatory genes (*Cox2, Ptges2,* and *Tnfa*)
1318 (C) and gut barrier genes (*Tjp1, Cld7, Ocln*, and *Muc2*) (D) in IECs of ABX-treated mice
1319 fed on RCD, MFD, and HFD.

1320 **E**: Venn diagram illustrating the common and unique species in the microbiomes of RCD,
1321 MBD, MFD, and HFD-fed mice.

1322 **F-H**: Volcano plots showing differentially enriched species across the conditions: MFD vs
1323 RCD, MBD vs RCD, and HFD and RCD. The size of the dots indicates the abundance of
1324 the species.

1325 **I**: Schematic illustration of the experimental workflow for *D. newyorkensis* treatment.

1326 **J**: Representative images of H&E stained colon tissue sections of control or *D.*
1327 *newyorkensis* treated mice with or without DSS insult.

1328 **K**: RT-qPCR analysis of *Ocln*, and *Hnf4a* in colon tissues of *D. newyorkensis* treated
1329 mice.

1330 **L**: Densitometric quantification of JNK and P38 blots shown in Figure 6O.

1331 Data are mean ± SEM, with statistical analysis by two-way ANOVA with Tukey's multiple
1332 comparison test (B, C, D, and K), one-way ANOVA with Tukey's multiple comparison test
1333 (L), and DESeq2 Padj <0.01 and absolute Log2 foldchange of >1 (F, G, and H). *$p < 0.05$,
1334 **$p < 0.01$, ***$p < 0.005$, ****$p < 0.001$.

1335 **Figure S7: Acetate induces the JNK2 pathway in the colonic epithelium to enhance**
1336 **gut barrier function.**

1337 **A**: Levels of propionate and butyrate in the fecal matter of control and *D. newyorkensis*
1338 treated mice.

1339 **B**: Representative images of colons from control or acetate-treated mice with and without
1340 1.5% DSS challenge.

1341 **C**: Western blot analyses of IECs isolated from control and acetate-treated mice showing
1342 p-P38 and total-P38 levels.

1343

1344

1345

Figure 1; Chongtham, et al.,

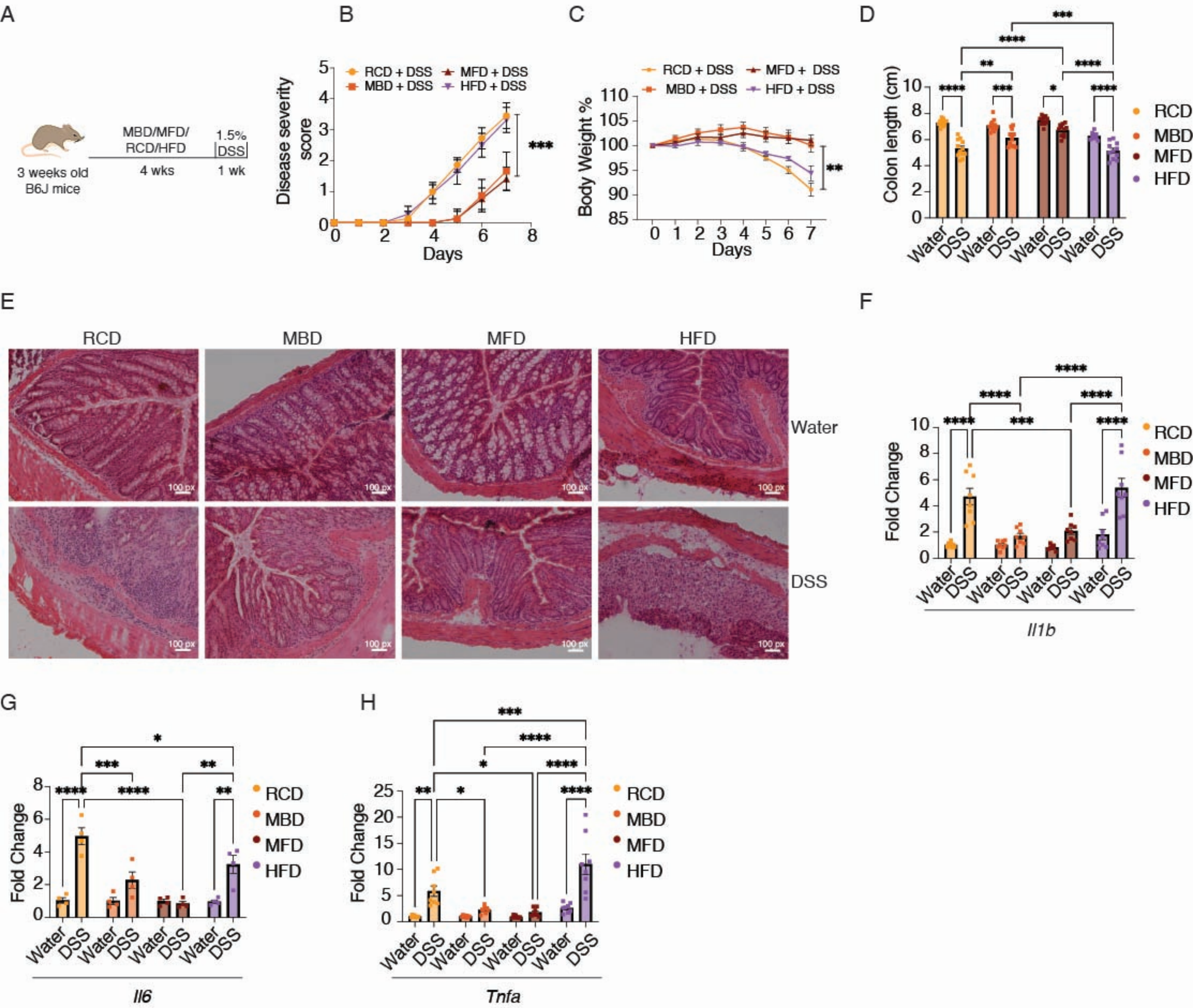

Figure 2; Chongtham et al.

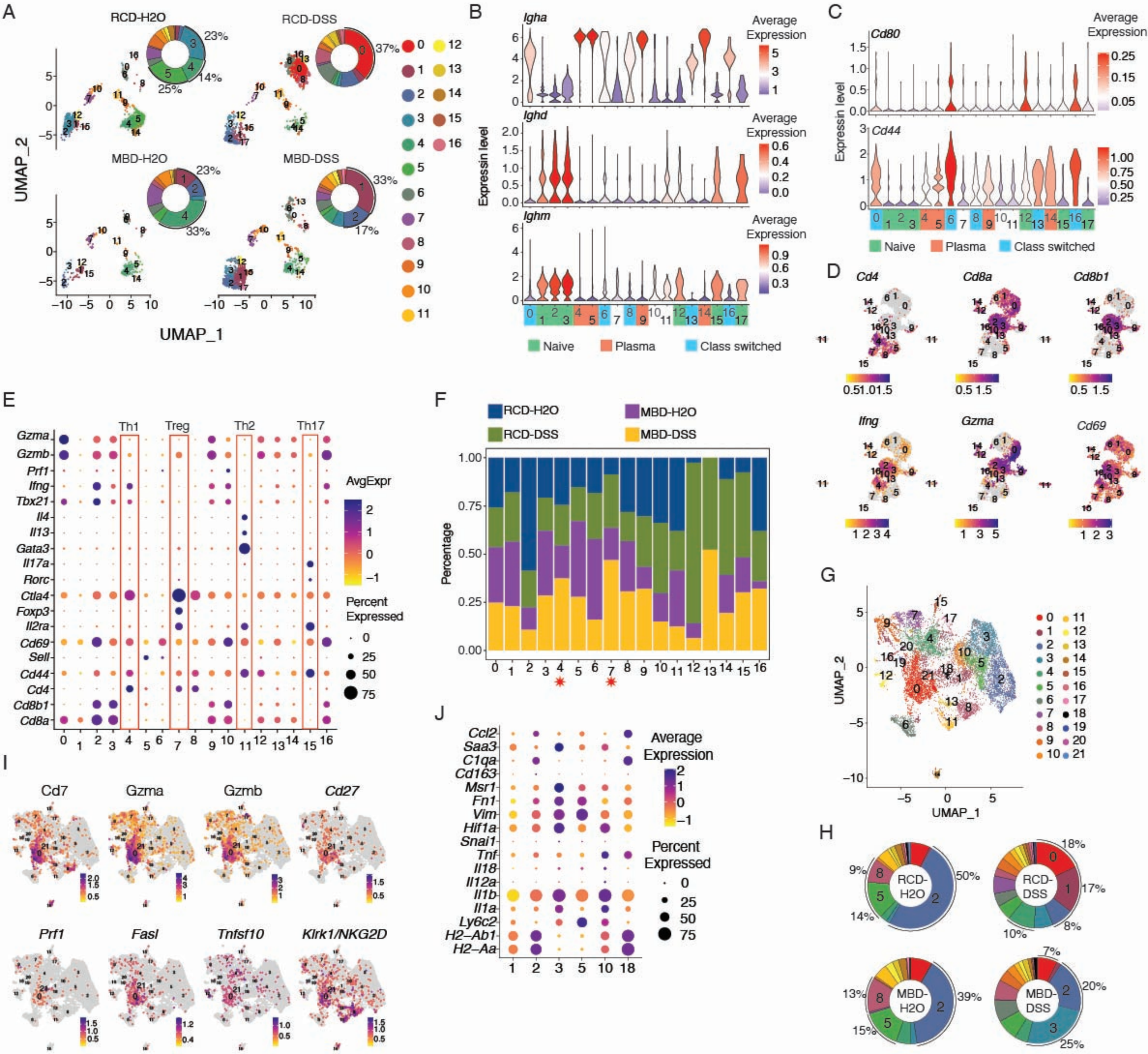

Figure 3; Chongtham et al.

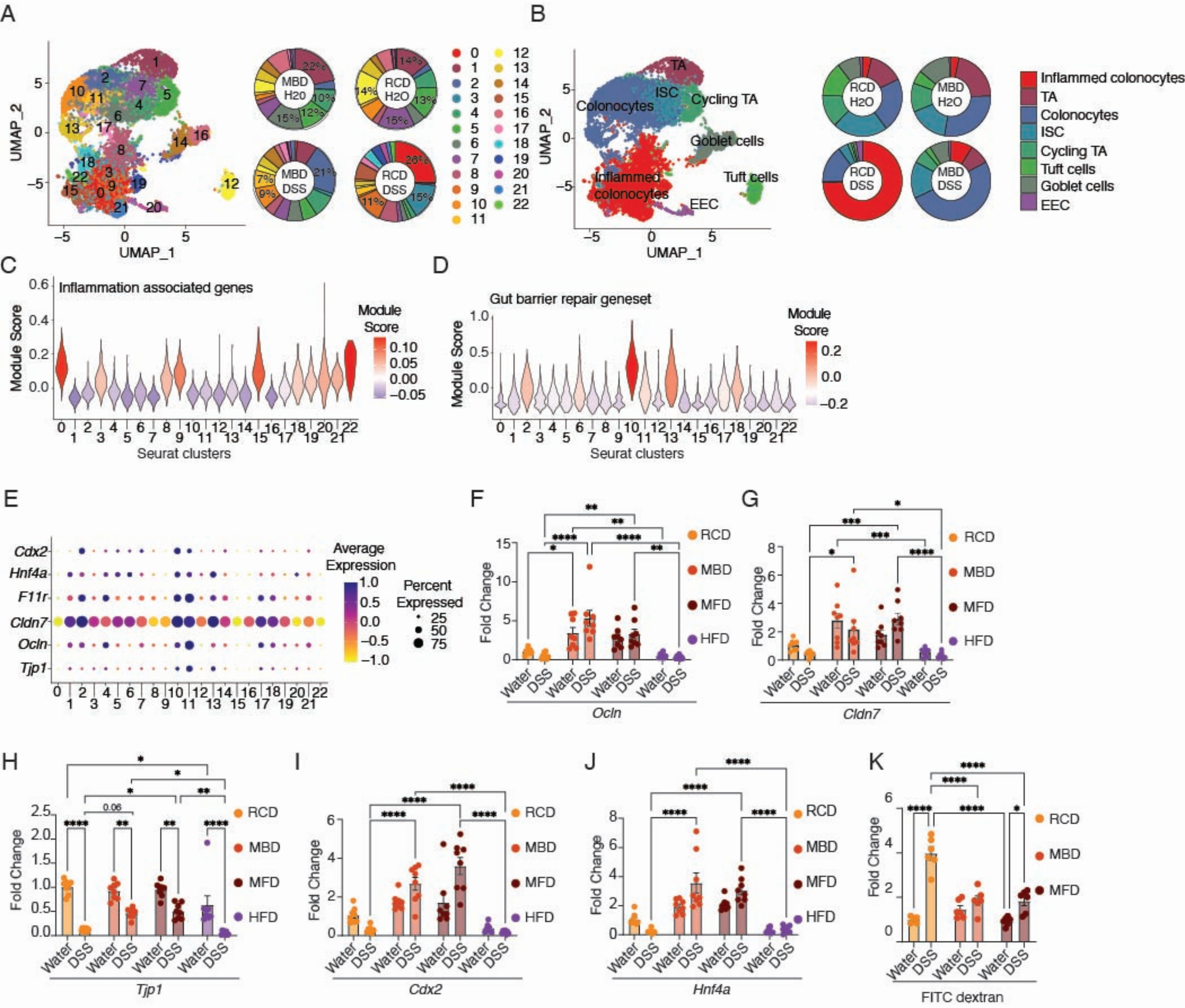

Figure 4; Chongtham et al.

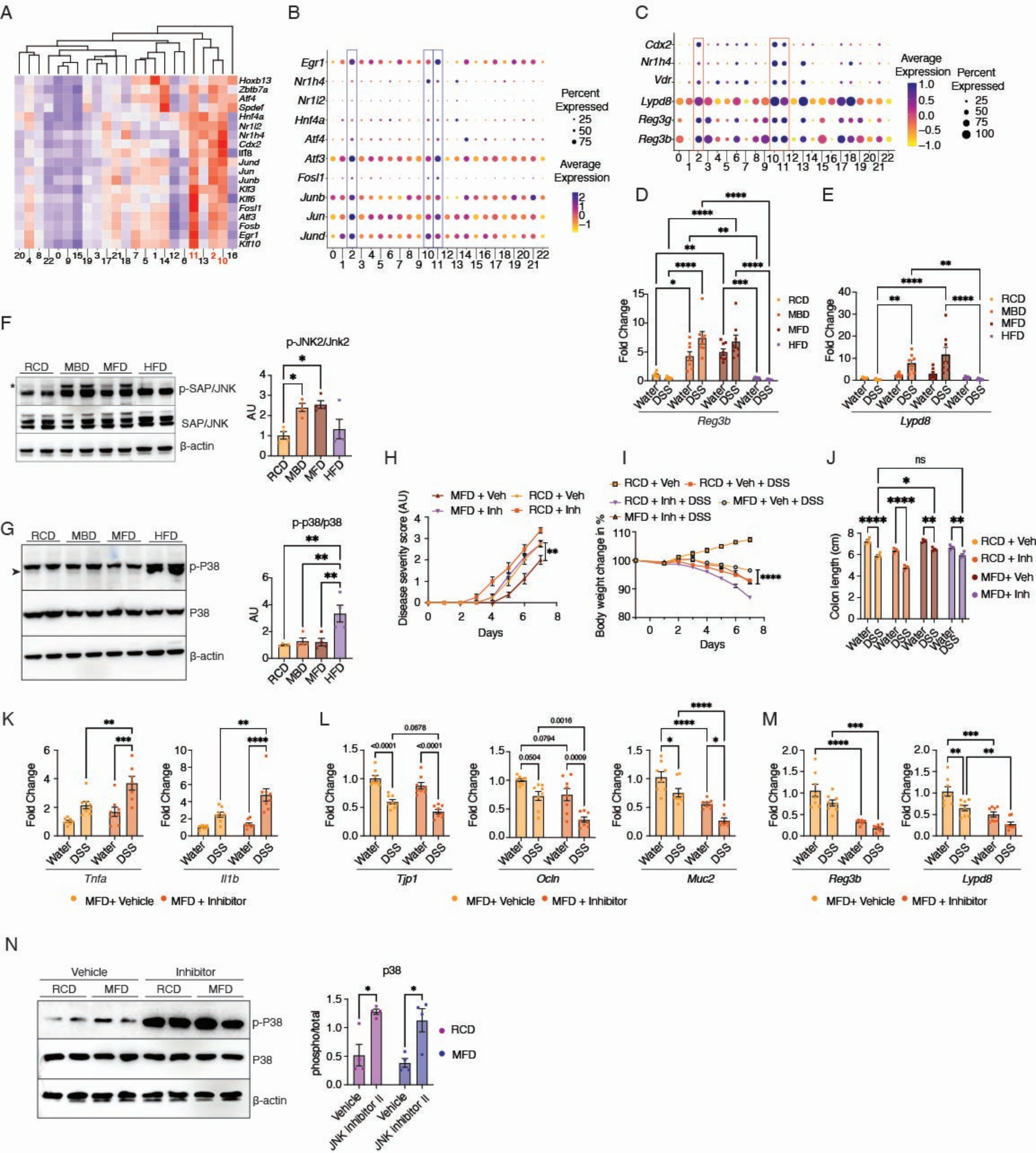

Figure 5, Chongtham et al.

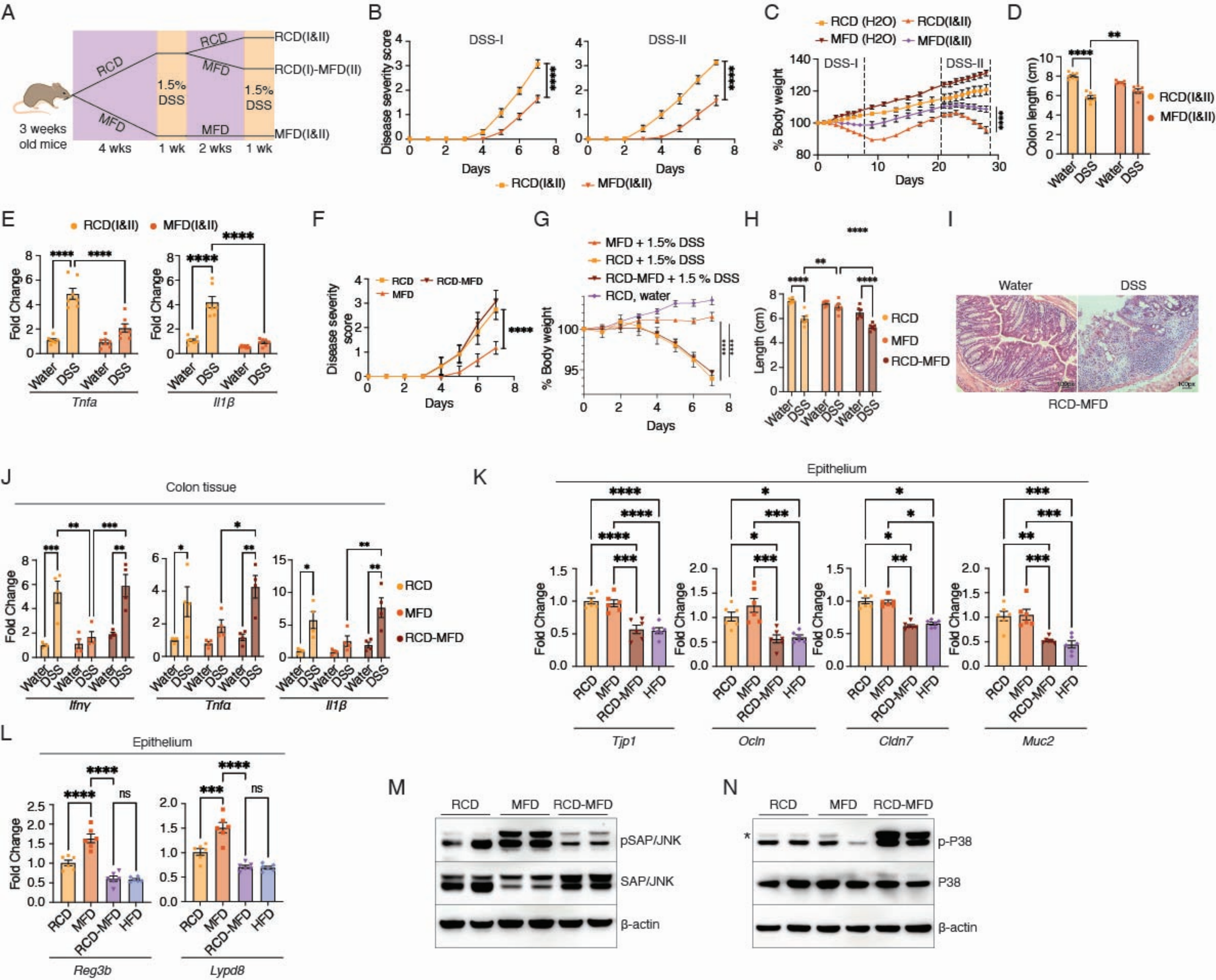

Figure 6; Chongtham et al.

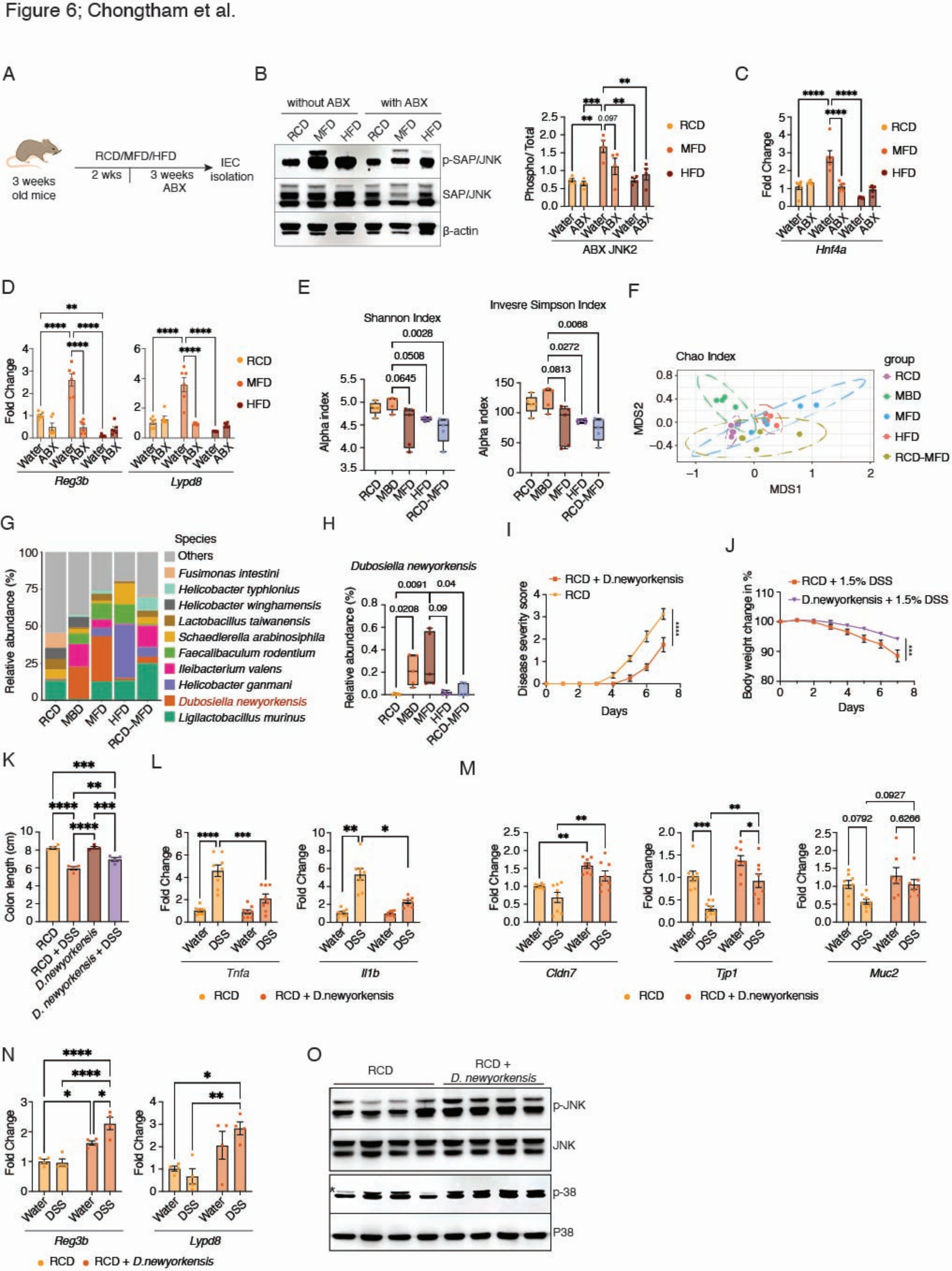

Figure 7; Chongtham et al.

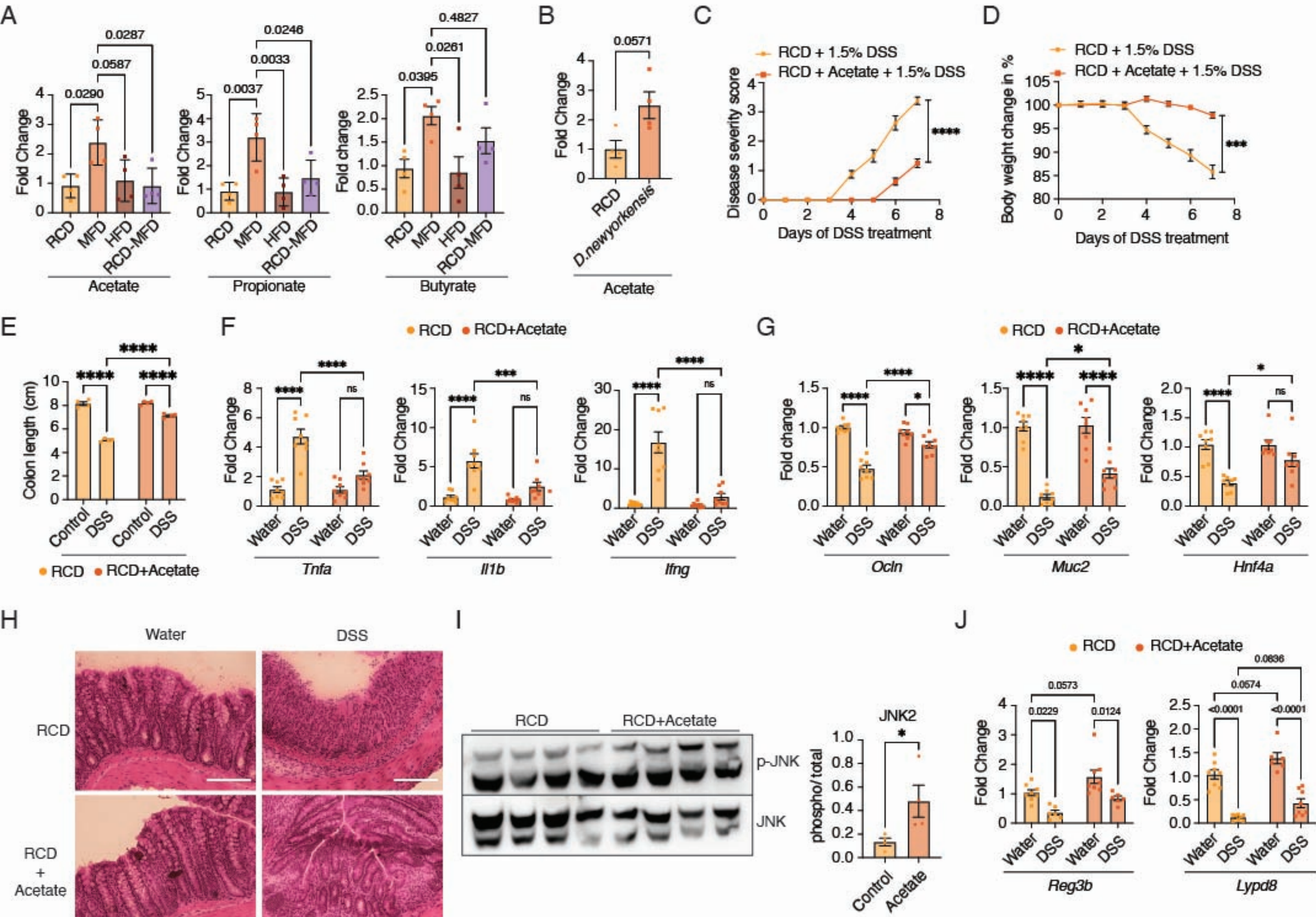

Figure S1; Chongtham et al.,

A

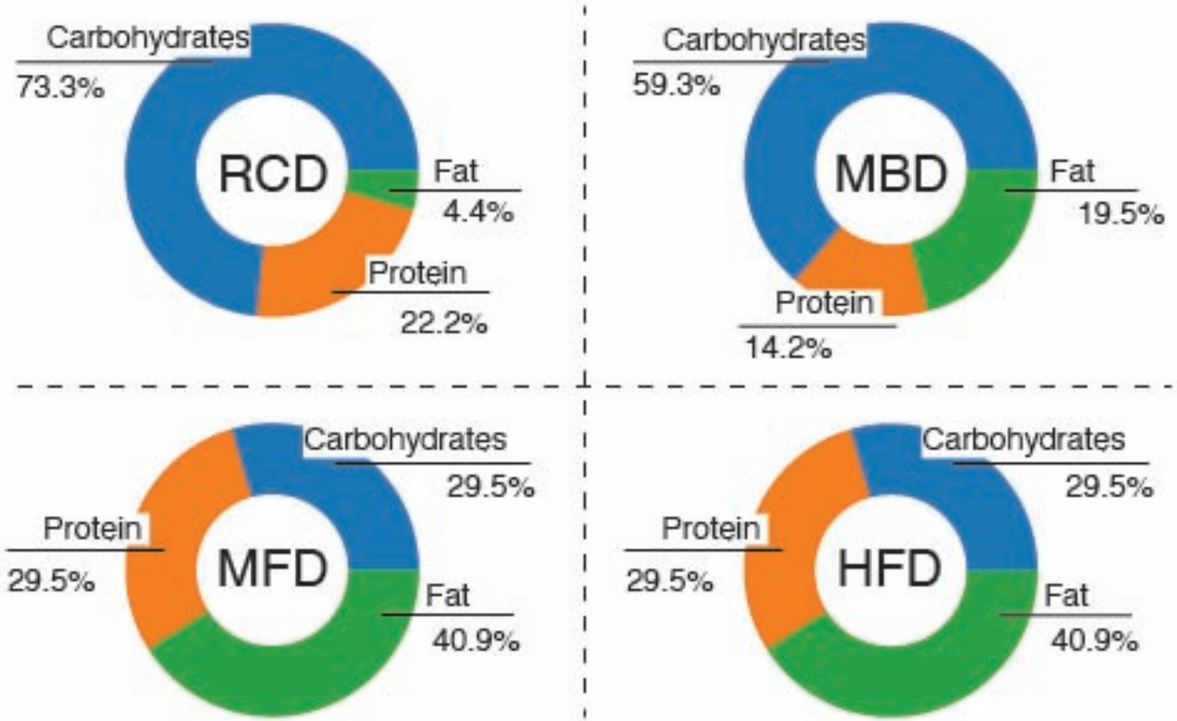

B

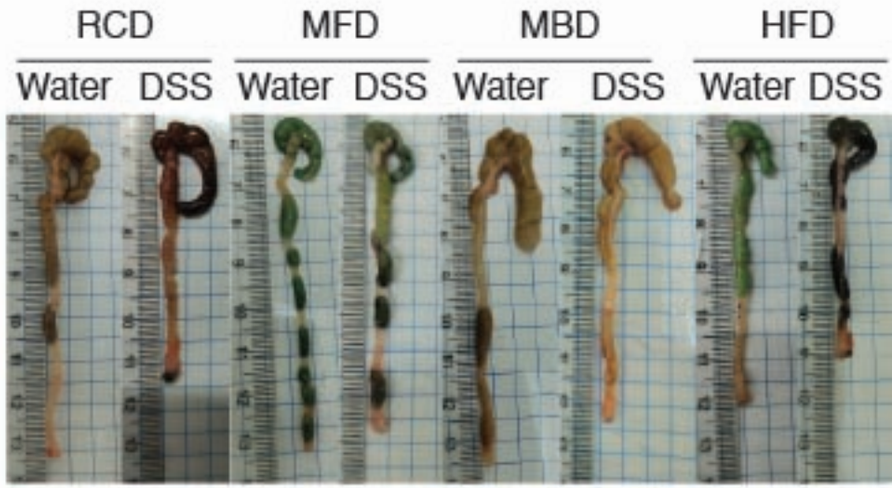

C

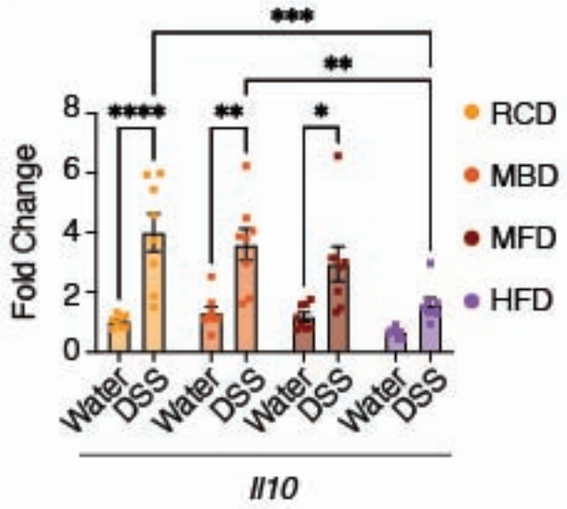

D

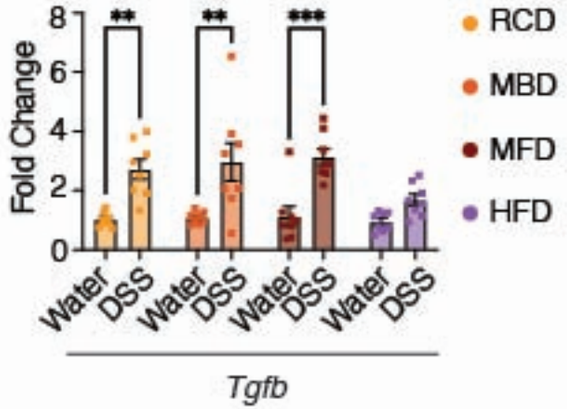

Figure S2; Chongtham et al.,

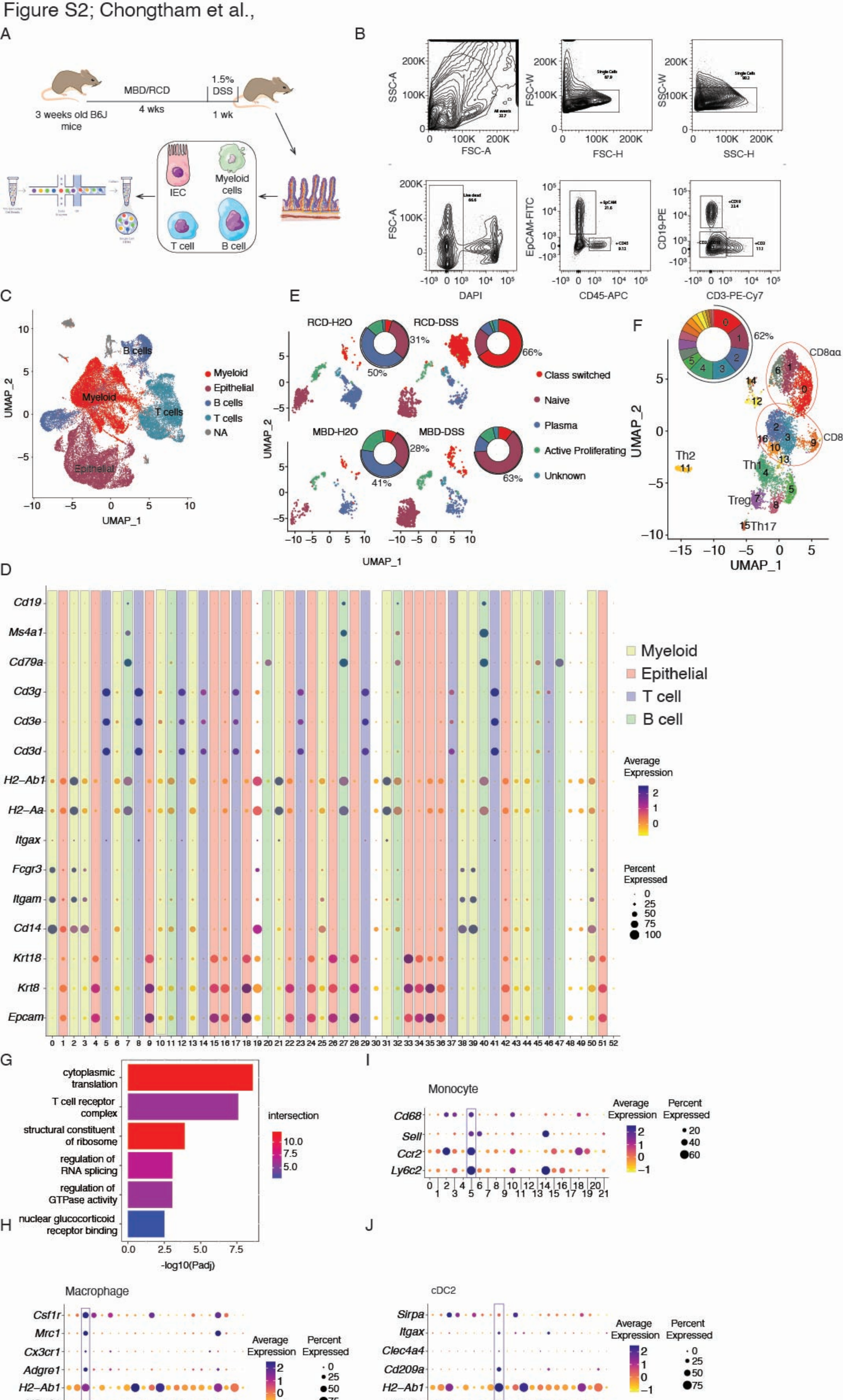

Figure S3; Chongtham et al.

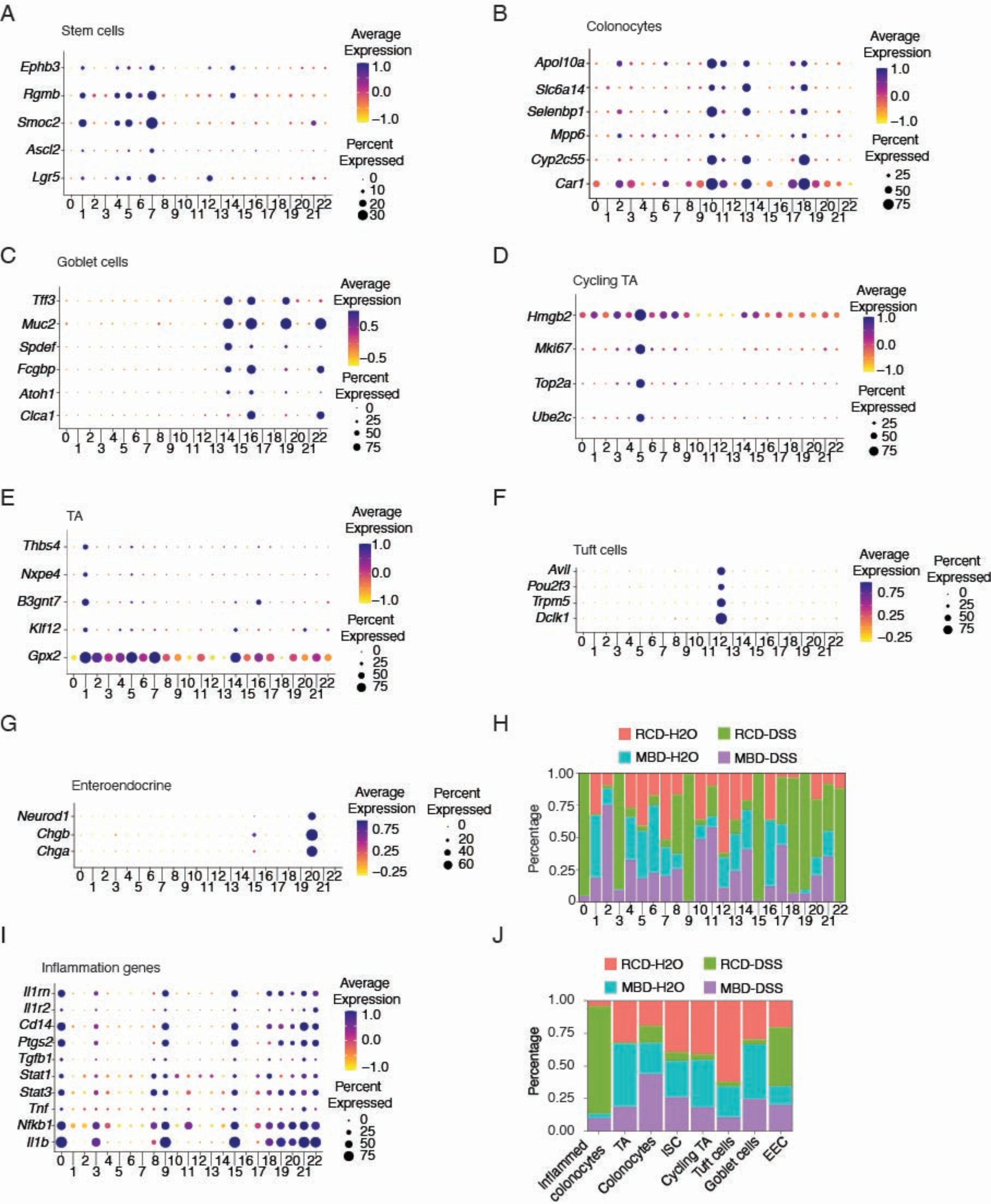

Figure S4, Chongtham et al.

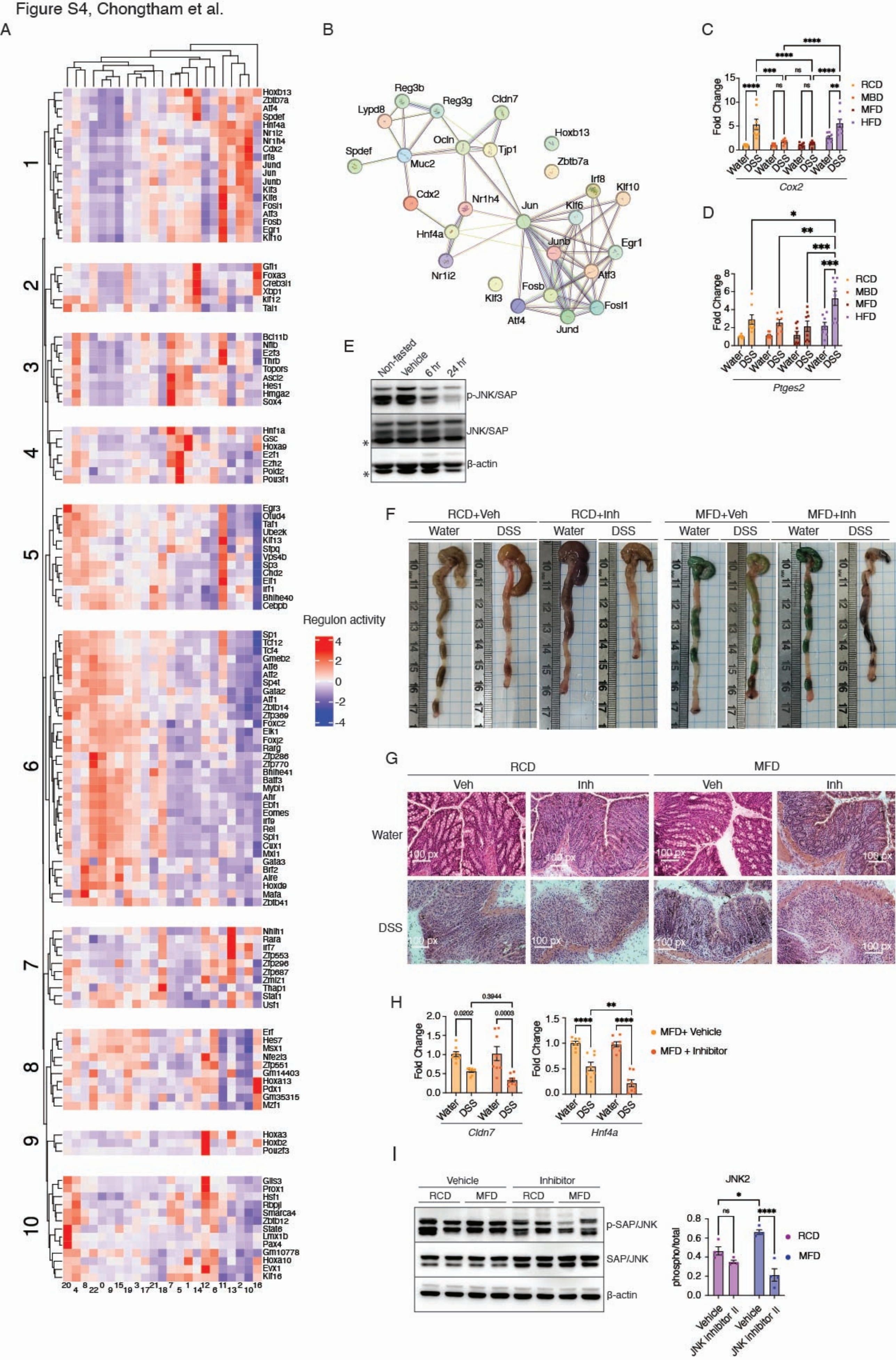

Figure S5, Chongtham et al.

A

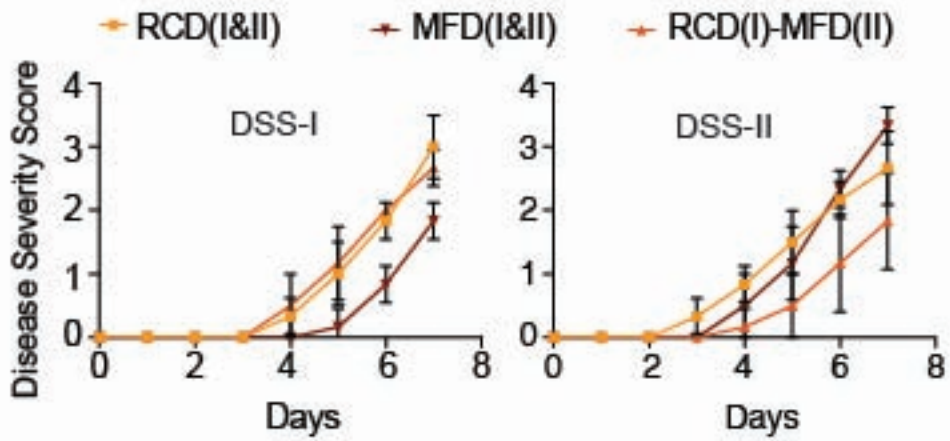

B

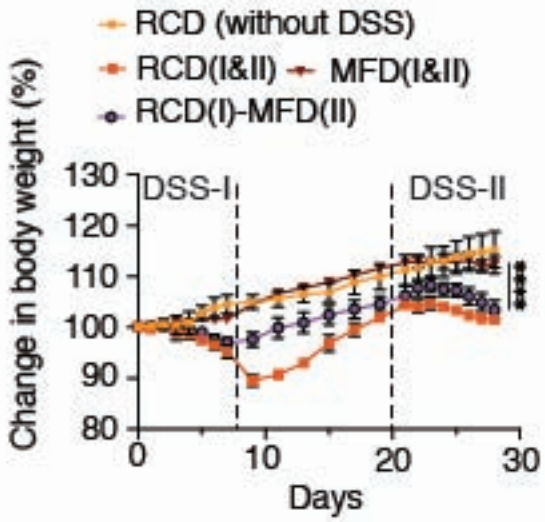

C

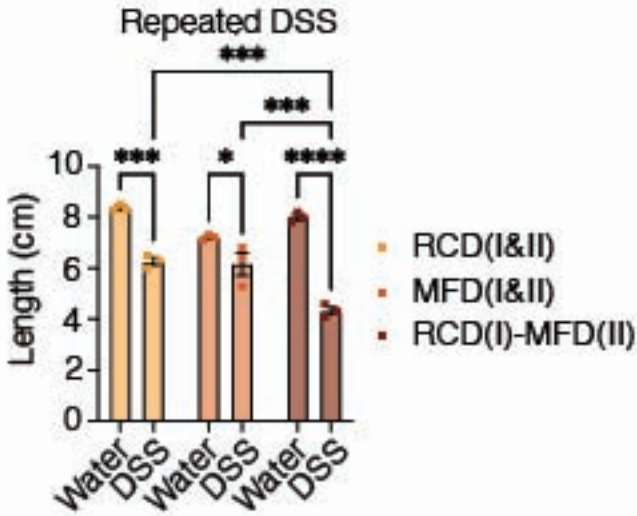

D

Figure S6; Chongtham et al.

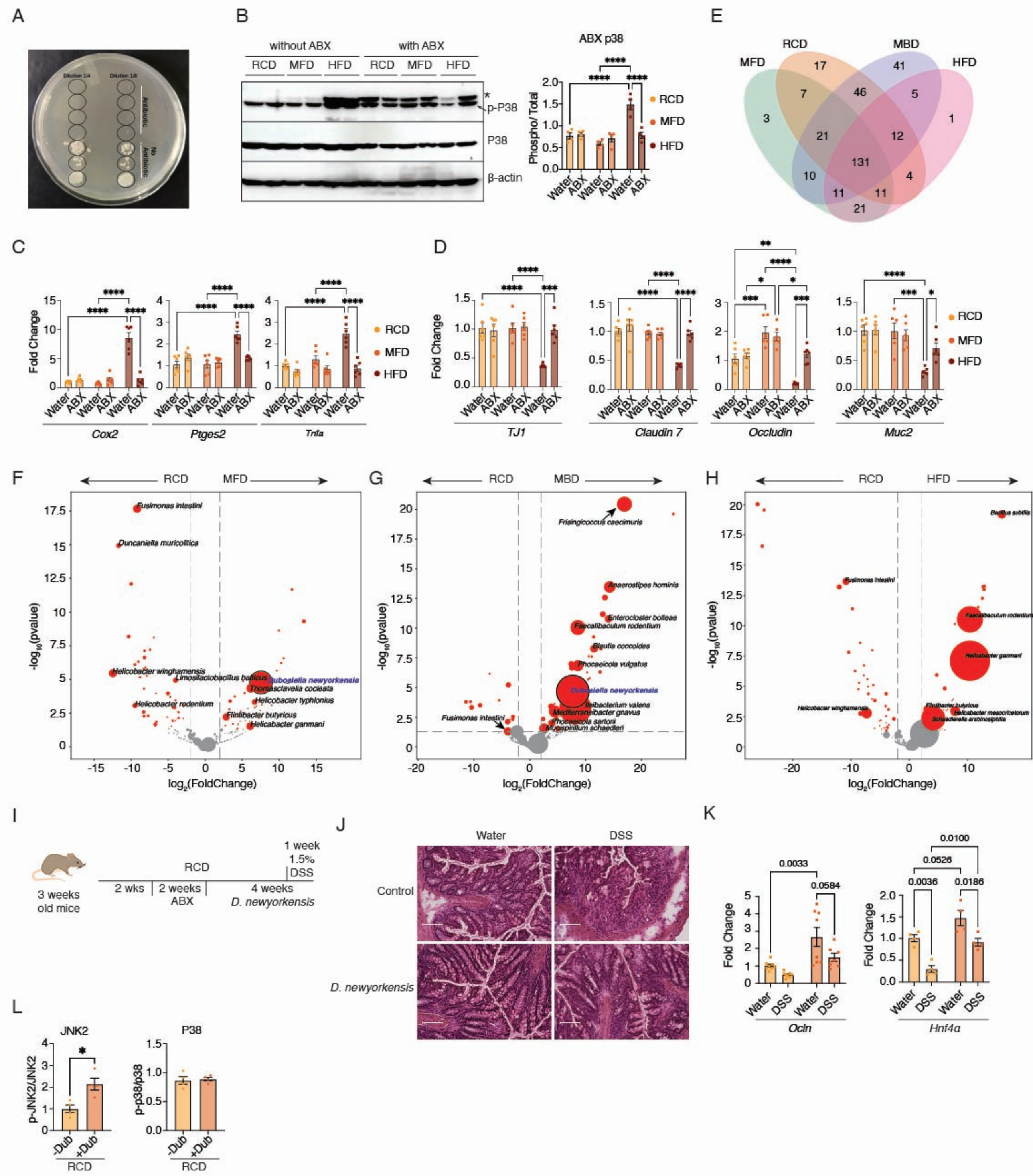

Figrue S7; Chongtham et al.

A

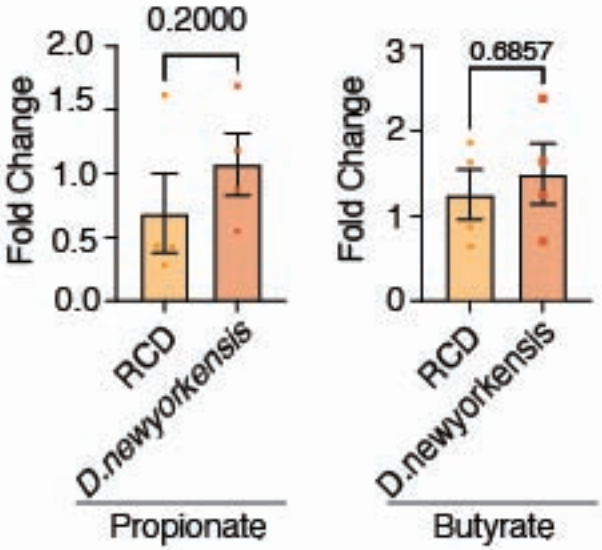

B

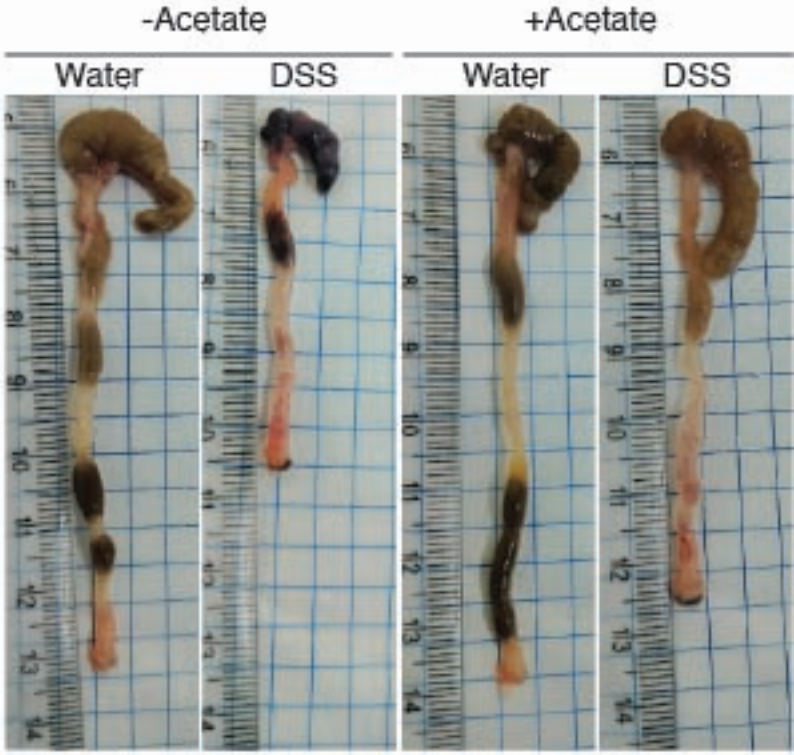

C

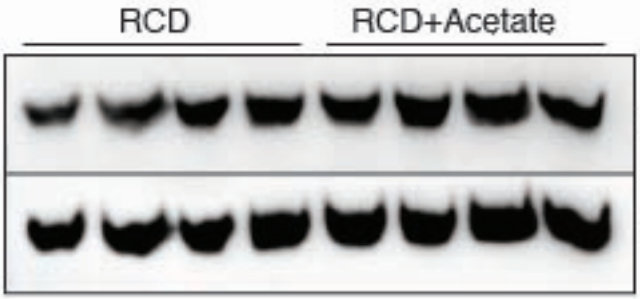

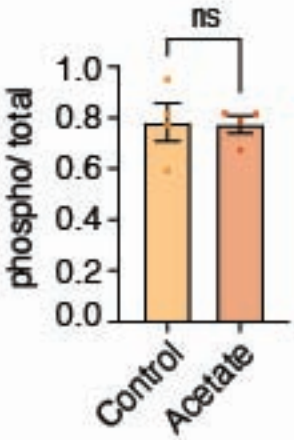

Table S1

	Chow		MBD		MFD		HFD	
	Altromin International		Nestle (Lactogen 2)		Research Diets		Research Diets	
	gm%	kcal%	gm%	kcal%	gm%	kcal%	gm%	kcal%
Protein	23.7	30	14	12	26	20	26	20
Carbohydrate	38	50	59	50	26	20	26	20
Fat	7	20	20	38	35	60	35	60
Energy Density	333.9 kcal/100g		469 kcal/100g		523.73 kcal/100g		521.2 kcal/100g	

Table S1: Macronutrient composition of the diets used in this study. A detailed description of the composition in given in the Supplemental Dataset 1

Table S2

Sl. No	Module	Gene list
1	Inflammation associated genes	*Ifng, Ifngr1, Ifngr2, Il10,Il12a, Il12b, Il12rb1, Il12rb2, Il13, Il17a, Il17f, Il18, Il18r1, Il18rap, Il1a, Il1b, Il2, Il21, Il21r, Il22, Il23a, Il23r, Il2rg, Il4, Il4r, Il5, Il6, Jun, Nfkb1, Rela, Rora, Rorc, S100a8, S100a9, Stat1, Stat3, Stat4, Stat6, Tgfb1, Tgfb2, Tgfb3, Tnf*
2	Gut barrier repair gene set	*Aqp8, Sult1a1, Hsd17b2, Padi2, Slc26a2, Selenbp1, Fam162a, Acads, Tst*

Table S2: List of genes used to calculate module scores.